Developmental Cognitive Neuroscience 48 (2021) 100883

Contents lists available at ScienceDirect

Developmental Cognitive Neuroscience

journal homepage: www.elsevier.com/locate/dcn

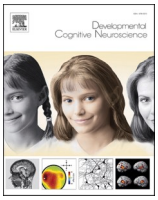

Restructuring of amygdala subregion apportion across adolescence

Claire E. Campbell [a,b], Adam F. Mezher [a,b], Sandrah P. Eckel [a], J. Michael Tyszka [c], Wolfgang M. Pauli [c], Bonnie J. Nagel [d], Megan M. Herting [a,*]

[a] Department of Preventive Medicine, Keck School of Medicine of University of Southern California, Los Angeles, CA, 90033, USA
[b] Neuroscience Graduate Program, University of Southern California, Los Angeles, CA, 90089-2520, USA
[c] Division of Humanities and Social Sciences, California Institute of Technology, Pasadena, CA, 91125, USA
[d] Departments of Psychiatry & Behavioral Neuroscience, Oregon Health & Science University, Portland, OR, 97239-3098, USA

ARTICLE INFO

Keywords:
Amygdala
Sex characteristics
Adolescent
Central amygdaloid nucleus
Basolateral nuclear complex
Corticomedial nuclear complex
Puberty

ABSTRACT

Total amygdala volumes develop in association with sex and puberty, and postmortem studies find neuronal numbers increase in a nuclei specific fashion across development. Thus, amygdala subregions and composition may evolve with age. Our goal was to examine if amygdala subregion absolute volumes and/or relative proportion varies as a function of age, sex, or puberty in a large sample of typically developing adolescents (N = 408, 43 % female, 10–17 years). Utilizing the in vivo CIT168 atlas, we quantified 9 subregions and implemented Generalized Additive Mixed Models to capture potential non-linear associations with age and pubertal status between sexes. Only males showed significant age associations with the basolateral ventral and paralaminar subdivision (BLVPL), central nucleus (CEN), and amygdala transition area (ATA). Again, only males showed relative differences in the *proportion* of the BLVPL, CEN, ATA, along with lateral (LA) and amygdalostriatal transition area (ASTA), with age. Using a best-fit modeling approach, age, and not puberty, was found to drive these associations. The results suggest that amygdala subregions show unique variations with age in males across adolescence. Future research is warranted to determine if our findings may contribute to sex differences in mental health that emerge across adolescence.

1. Introduction

The amygdala is a collection of nuclei located in the medial temporal lobe, with extensive connections to the cerebral cortex (Amaral and Price, 1984; Barbas and De Olmos, 1990; Ghashghaei and Barbas, 2002). The heterogeneous structure and function of the amygdala nuclei play a vital role in mediating a number of cognitive, affective, and motivational processes (Baxter and Murray, 2002; Hariri et al., 2002; Meyer--Lindenberg et al., 2005; Raznahan et al., 2011; Bzdok et al., 2013; Tottenham and Gabard-Durnam, 2017). Cytoarchitecture and lesion studies have helped determine how these diverse groupings of amygdala neurons mediate specific processes (Krettek and Price, 1978; Amaral and Price, 1984; Ghashghaei and Barbas, 2002; Amunts et al., 2005; Solano-Castiella et al., 2011). Previous studies have shown the basal and lateral nuclei process high-level sensory input and emotional regulation (Sananes and Davis, 1992; Wan and Swerdlow, 1997; Schoenbaum et al., 1999), while the central nucleus is involved in reward and aversive learning (Killcross et al., 1997; Baxter and Murray, 2002). Moreover, the paralaminar nucleus of the amygdala contains neurons that continue to mature and migrate into adulthood (Amaral and Price, 1984; Bernier et al., 2002; Tosevski et al., 2002; deCampo and Fudge, 2012); this region's potential for regional neural plasticity (deCampo and Fudge, 2012) may be involved in modulating changes in nuclei size and thus the restructuring of amygdala composition.

When treating the amygdala as a singular unit, total amygdala volumes continue to increase from childhood to young adulthood, with distinct developmental patterns seen based on sex and pubertal stage. In one cross-sectional study of 10–14 year-olds (N = 80) it was found that greater pubertal development was associated with larger amygdala bilaterally regardless of sex (Bramen et al., 2011), while another cross-sectional study examining 4–18 year-olds (N = 99) found that a larger left amygdala was associated with greater pubertal development, but only in males (Giedd et al., 1996). Moreover, longitudinal studies found that amygdala development shows a nonlinear relationship with

* Corresponding author at: Keck School of Medicine of University of Southern California, Departments of Preventive Medicine, 2001 N. Soto, Los Angeles, CA, 90089, USA.
E-mail address: herting@usc.edu (M.M. Herting).

https://doi.org/10.1016/j.dcn.2020.100883
Received 28 May 2020; Received in revised form 5 November 2020; Accepted 13 November 2020
Available online 11 December 2020

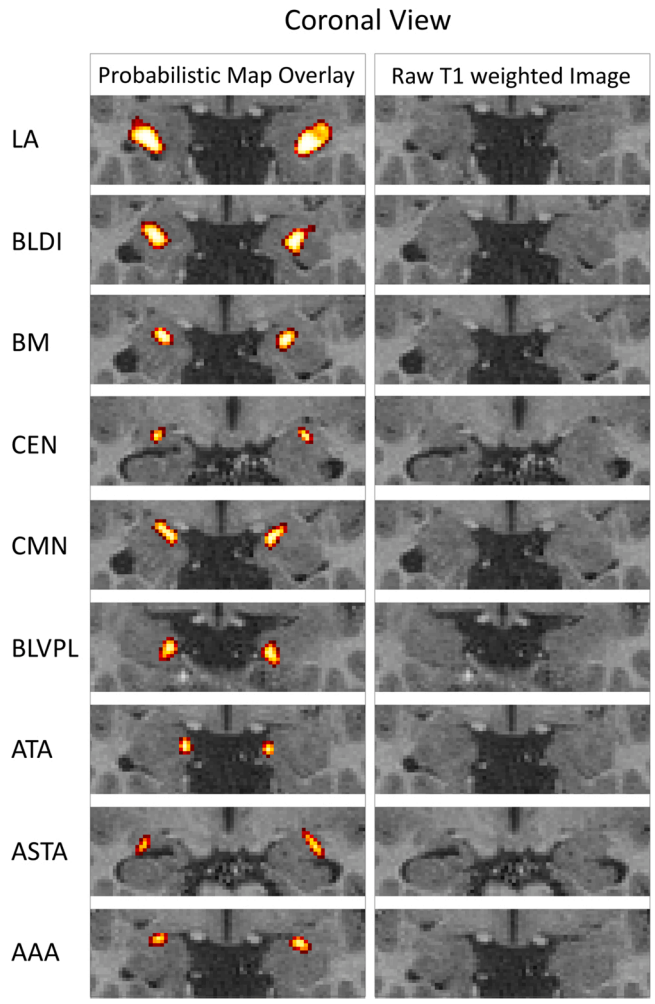

Fig. 1. Probabilistic map of each amygdala subregion in a representative adolescent. Structural MRI with the left column showing the probabilistic maps of the 9 bilateral subregions shown in the coronal view (thresholded at probabilistic value of .15 for visualization purposes) and the right column showing the raw T1 weighted image in the same coronal slice. Key: LA, lateral nucleus; BLDI, basolateral dorsal and intermediate subdivision; BLVPL, basolateral ventral and paralaminar subdivision; BM, basomedial nucleus; CMN, cortical and medial nuclei; CEN, central nucleus; AAA, anterior amygdala area; ATA, amygdala transition area; ASTA, amygdalostriatal transition area.

smaller volumes at younger ages, and with males having larger volumes as compared to females (Wierenga et al., 2014; Herting et al., 2018). In longitudinal studies examining pubertal status relationship with amygdala development, the left amygdala was found to be larger in males as compared to females, while the right amygdala varied depending on sex, testosterone levels, Tanner Stage, and age in 10–14 year-olds (N = 126) (Herting et al., 2014). Another study of 8–29 year-olds (N = 271) found age was a better predictor of amygdala volumes in females, but male amygdala volumes were best predicted by testosterone as compared to age or puberty (Wierenga et al., 2018). In another longitudinal study of 7–20 year-olds (N = 275), they found age added to a pubertal model explained additional variance in amygdala volumes for both males and females (Goddings et al., 2014). Together these studies strongly suggest that the amygdala continues to develop across adolescence. Yet, treating the amygdala as a single structure may mask the potential specificity of age-related anatomical changes within structurally and functionally distinct amygdala subnuclei. For example, a recent postmortem study (N = 24 neurotypical brains, ages 2–48 years) found that neuron numbers increase in the amygdala but do so in a nucleus specific manner (Avino et al., 2018), suggesting that regionally specific neuronal increases may contribute to age and/or puberty related differences in amygdala subregion volumes and/or subregional apportionment across childhood and adolescence.

Accordingly, our study aimed to quantify both the absolute volumes as well as the relative proportion, or the *relative volume fraction (RVF),* of amygdala subregions in a large cross-sectional sample of 408 children and adolescents (n = 177 females, ages 10–17 years) as well as examine if these patterns varied as a function of age, sex, or pubertal status. While previous amygdala atlases have been limited as they have been created by *ex vivo* brains from small samples of elderly, male individuals (Amunts et al., 2005; Saygin et al., 2017), we implemented a newly developed high-resolution probabilistic atlas, known as the CIT168, which was created using in vivo MRI data from 168 (50 % female) healthy young adult brains (Tyszka and Pauli, 2016; Pauli et al., 2018). Using this approach, we segmented the amygdala into nine bilateral regions of interest (ROIs), including the lateral nucleus (LA), basolateral dorsal and intermediate subdivision (BLDI), basolateral ventral and paralaminar subdivision (BLVPL), basomedial nucleus (BM), cortical and medial nuclei (CMN), central nucleus (CEN), anterior amygdala area (AAA), amygdala transition areas (ATA), and amygdalostriatal transition area (ASTA) (Fig. 1). Building on previous research (Rollins and King, 2000; Baxter and Murray, 2002; Herting et al., 2014; Wierenga et al., 2014; Janak and Tye, 2015; Tyszka and Pauli, 2016; Herting et al., 2018; Wierenga et al., 2018), we then examined how age, sex, and pubertal status were associated with subregion volumes as well as the relative proportion of each subregion within the amygdala in adolescents. Given that the basolateral nucleus increases innervation with the prefrontal cortex during adolescent neurodevelopment (Cunningham et al., 2002) and the paralaminar's potential for postnatal neuroplasticity (deCampo and Fudge, 2012), we hypothesized that lateral, basal, and paralaminar subregions would be larger, as well as occupy a larger proportion of the amygdala – regardless of an overall increase in amygdala volume since other subregions may reduce in size – as a function of age and/or puberty across adolescence. Moreover, we also predicted that given the non-linear developmental patterns seen in adolescence (Wierenga et al., 2014; Herting et al., 2018), there would be non-linear age/puberty associations with these above-mentioned amygdala subregions that differ between the sexes, with more variability seen in males. Ultimately, understanding how the human amygdala associates and develops throughout adolescence may help discern developmental changes seen in social-emotional and reward-related behavior, as well as identify risk factors for mental health disorders.

2. Materials and methods

2.1. Participants and measures

This study incorporated cross-sectional data from 408 adolescents (n = 177 females), ages 10–17 years (Supporting Fig. 1), from ongoing research studies at Oregon Health & Science University. A comprehensive telephone interview was conducted to determine eligibility for all participants, and written consent and assent were obtained from each participating adolescent and at least one of their biological parents. All participants were right-handed and free of neurological, neurodevelopmental, and/or psychological diagnoses based on the DISC Predictive Scales (Shaffer et al., 2000). Subjects were also excluded if they: obtained head trauma; had serious medical problems; reported learning disabilities; used any medications that affected their central nervous system; consumed >10 lifetime alcoholic drinks, >2 alcoholic drinks on one occasion, >10 lifetime uses of marijuana, >4 lifetime uses of cigarettes, and any other drug use history; had maternal alcohol use of 4 drinks per occasion or 7 drinks per week or other drugs during pregnancy; parental history of a psychotic illness; inadequate English skills; sensory issues; non-removable metal in their body; pregnancy. The prior exclusionary criteria can be found in greater detail in cited papers

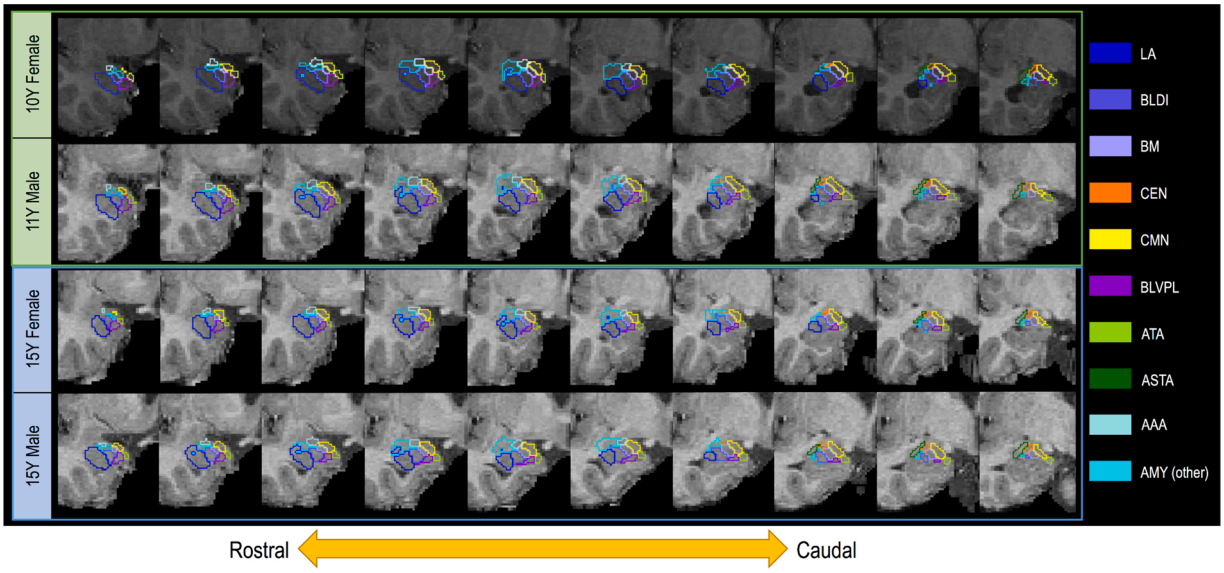

Fig. 2. Outline of CIT168 segmentation on coronal slices through entire rostral-caudal view of the amygdala in the right hemisphere for four representative subjects. A maximum likelihood label was created for each subregion of the amygdala by creating a label based on a simple competition between probabilistic labels with a thresholded probabilistic value of .3 for visualization purposes; slices (1 mm) are sequential (no gap).

(Alarcon et al., 2015; Scheuer et al., 2017; Morales et al., 2018) and in Supporting Information: Exclusionary Criteria.

Based on prior research (Rollins and King, 2000; Baxter and Murray, 2002; Herting et al., 2014; Wierenga et al., 2014; Janak and Tye, 2015; Tyszka and Pauli, 2016; Herting et al., 2018; Wierenga et al., 2018), we considered three primary biological and physical factors for each participant: age, sex, and pubertal status. Pubertal status was determined by self-report using the Pubertal Development Scale (PDS) (Petersen et al., 1988), with scores for each of the 5 questions ranging from 1 (not started) to 4 (development seems complete). Scores across the items were averaged to a single comprehensive score. Based on the literature, we also identified two important covariates, including social economic status (SES) (Brito and Noble, 2014) and body mass index (BMI) (Perlaki et al., 2018). SES was assessed utilizing the Hollingshead Four-Factor Index of Socioeconomic Status-Child (Hollingshead, 1975) and BMI using the Centers for Disease Control and Prevention's BMI Percentile Calculator for Child and Teen English Version (http://nccd.cdc.gov/dnpabmi/Calculator.aspx) by providing participant birth date, date of measurement, sex, height (to nearest 0.1 cm) and weight (to nearest 0.1 kg); subjects were removed if they did not have BMI values (Supporting Fig. 2). BMI z-scores (BMIz), which correspond to growth chart percentiles, were then calculated to reflect the relative weight of the individual using the appropriate reference standard based on the individual's age and sex (Must and Anderson, 2006).

2.2. MRI data collection and preprocessing

A whole-brain T1-weighted MRI scan was acquired for each participant on the same 3 T MRI system (Magnetom Tim Trio, Siemens Medical Solutions, Erlangen, Germany) using a 12-channel head coil at the Oregon Health & Science University's Advanced Imaging Research Center (TR =2300 ms, TE =3.58 ms, TI =900 ms, flip angle = 10°, 256 × 240 matrix, voxel size = 1.0 mm x 1.0 mm x 1.1 mm). Raw images were visually quality checked for motion and given a rating of 1 (pass), 2 (review), or 3 (fail) (Backhausen et al., 2016); for details, see Supporting Fig. 2. Using the Functional Magnetic Resonance Imaging of the Brain Software Library (FSL) version 5.0 (Smith et al., 2004; Woolrich et al., 2009; Jenkinson et al., 2012). Each brain image was first reoriented to standard orientation using FSL's *fslreorient2std* function. Images were then automatically cropped to reduce lower head and neck using FSL's *robustfov* tool and rigid-body AC-PC aligned. Using the *antsBrainExtraction* function from the Advanced Normalization Tools (ANTs, Version 2.1.0.post691-g9bc18) (Avants et al., 2011), each image was skull-stripped to allow for an N4 Bias Field Correction (Tustison et al., 2010) on the whole-brain image.

2.3. Probabilistic amygdala volumes and relative volume fractions (RVF)

Details of the in vivo amygdala probabilistic atlas construction, validation, estimates of individual differences, and comparison with previous atlas' have been previously reported (Tyszka and Pauli, 2016; Pauli et al., 2018). As previously published (Herting et al., 2020), we adapted this technique to allow for each youth's image to be registered to the CIT168 atlas using a B-spline bivariate symmetric normalization (SyN) diffeomorphic registration algorithm from ANTs version 2.2 (Avants et al., 2007). Applying the inverse diffeomorphism mapped the CIT168 probabilistic atlas labels to the individual space of each participant, yielding probabilistic ROIs for left and right total amygdala and the following nine subregions: lateral nucleus (LA); dorsal and intermediate divisions of the basolateral nucleus (BLDI); ventral division of the basolateral nucleus and paralaminar nucleus (BLVPL); basomedial nucleus (BM); central nucleus (CEN); cortical and medial nuclei (CMN); amygdala transition areas (ATA); amygdalostriatal transition area (ASTA); and anterior amygdala area (AAA). Descriptions of each subregion can be found in Supporting Table 1. The quality of all amygdala segmentations was confirmed visually (A.F.M.). Total ROI volumes were estimated by summation over the entire brain of voxel volumes weighted by the probability that a voxel belonged to the ROI. This approach differs from deterministic voxel summation following application of an arbitrary probability threshold (typically $p > 0.5$) in that uncertainty about the true extent of the ROI continues to be accurately represented in the resulting volume estimate. In addition to the absolute volume of the whole amygdala and each ROI generated from the CIT168 atlas, the fractional volume of each ROI within the amygdala was estimated relative to the total amygdala volume in each hemisphere, referred to subsequently as the relative volume fraction (RVF) for a given ROI.

Although the CIT168 atlas labels were delineated in high CNR template images, the amygdala nuclei in individual T1-weighted images have much lower CNR. The accuracy of volume estimates of amygdala

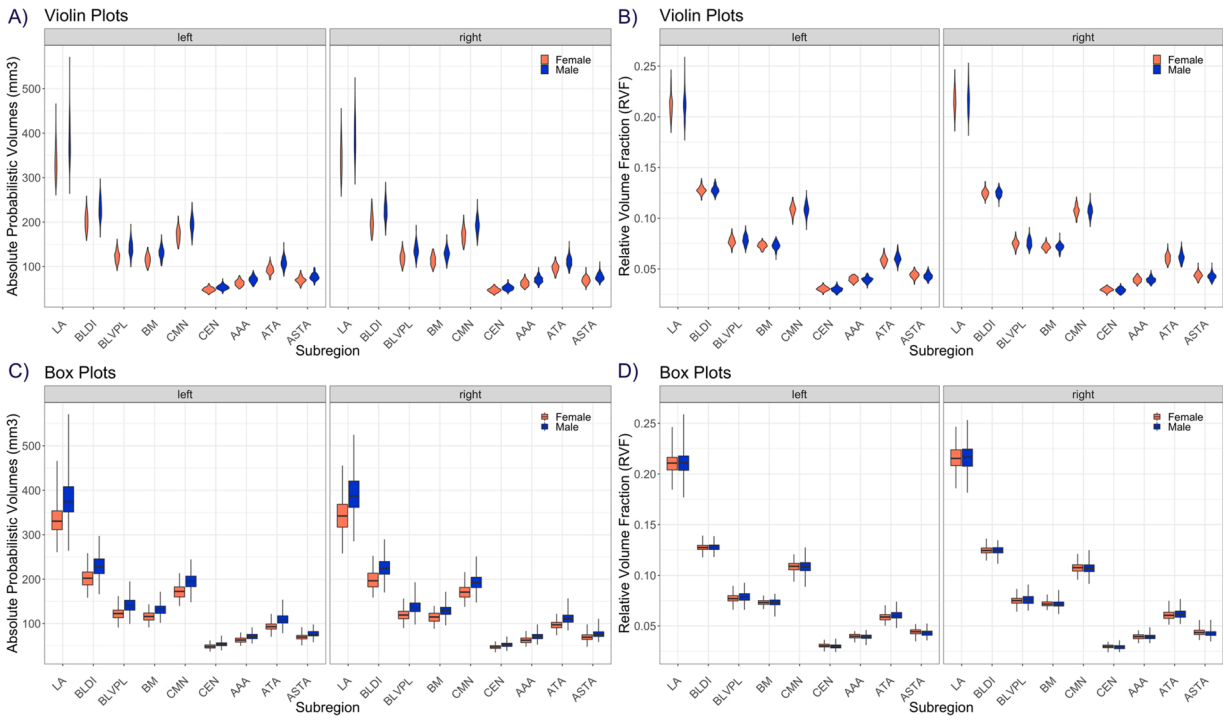

Fig. 3. Amygdala subregion volumes and relative volume fractions in adolescent males and females. Violin plots demonstrate the full distribution of the data by sex, by showing the frequency and extent of variation for each subregion for both A) absolute probabilistic volumes (mm^3) and B) relative volume fraction (RVF; proportional to total amygdala volume) for each of the 9 bilateral amygdala subregion ROIs. Box plots demonstrate the median, first and third quartiles, and the upper and lower whiskers (3.5 times the interquartile range) for both C) absolute probabilistic volumes (mm^3) and D) relative volume fraction (RVF; proportional to total amygdala volume).

subregions is heavily dependent on the accuracy of the SyN diffeomorphic registration between the high-CNR CIT168 space and the low-CNR individual space, where subnuclear boundaries become very indistinct to a human observer when viewed in 2D sections. Prior work modeling the accuracy of volume estimates in low CNR scenarios (Tyszka and Pauli (2016) suggests the implementation of the SyN diffeomorphic algorithm used in this study is relatively robust at CNRs of 1.0 and higher. This robustness is likely a consequence of the registration cost function drawing information from a local volume (approximately 4 voxel radius) to optimize the local deformation. Consequently, any subject with an intra-amygdala CNR less than 1.0 in either the right or left amygdala was excluded from further analyses (Supporting Fig. 2). Intra-amygdala CNR was estimated as follows: 1. The intensity contrast within the amygdala was estimated from the interquartile range (IQR) of intensities within the entire amygdala from each subject's T1-weighted image. 2. The standard deviation (SD) of the noise was estimated from the residual signal obtained when the T1-weighted atlas template image was subtracted from each subject's T1-weighted image. 3. The CNR was estimated as the ratio of the IQR to noise SD within the amygdala. The group mean SD over all subjects of residual signal within the amygdala was 24 for the right and 25 for the left hemisphere. The mean lower and upper quartile intensities within the amygdala were 278 and 311 (IQR = 33) for the right hemisphere and 277 and 310 (IQR = 33) for the left hemisphere. The average CNR was 1.4 for the amygdala in both hemispheres in our sample, suggesting the current study has sufficient CNR necessary to support robust amygdala subregion volume estimation when using SyN diffeomorphic registration (Tyszka and Pauli, 2016).

A 2-Dimensional visual representation of the probabilistic maps of each amygdala subregion segmentation on a representative subject can be seen in Fig. 1. To fully demonstrate the CIT168 segmentation, overlay images of coronal slices through the entire rostral-caudal extent of the amygdala with boundary outlines for each ROI is also presented for four subjects in Fig. 2. The subjects were randomly chosen to cover the distributions of our age range, including 1 male and 1 female from both the early and older adolescent periods. We also provide probabilistic estimates at the group level for a subset (N = 52) of our sample in Supporting Fig. 3.

2.4. Statistical analysis

Data were analyzed in R (version 3.5.1). To determine if there were relationships between our independent variables (age and puberty) and our covariates, as well as if these relationships significantly varied between the sexes, we performed a series of linear regressions (M1). Specifically, we examined if: age or PDS (and its interaction with sex) predicted intracranial volume (ICV), BMIz, and SES.

$$M1: \ Y = \beta_0 + \beta_1 X_1 + \beta_2 Male + \beta_3 X_1 \times Male + \varepsilon$$

Violin plots were utilized to visualize the full distribution and frequency of our data by sex for both the absolute probabilistic volumes and the RVFs of each ROI (Fig. 3) since previous research has shown brain volume distributions vary by sex (Wierenga et al., 2018, 2020); we also display box plots to help obtain a complete picture of the data (Fig. 3).

To examine if absolute probabilistic volumes and composition (i.e. proportional volumes or RVFs) related to age, sex, and pubertal status, we employed a Generalized Additive Mixed Model (GAMM) implemented by the *mgcv* package (version 1.8–24 in R version 3.5.1, R Core Team, 2018). Given that this developmental period shows non-linear subcortical brain volume growth patterns (Wierenga et al., 2014; Herting et al., 2018), a GAMM approach was chosen as it allows for data-driven estimation of non-linear associations (with linearity as a special case), using 'smooth' functions, s(), in place of linear terms. To examine the association between age and amygdala probabilistic volumes and composition (RVF), as well as determine if these associations vary by sex, each ROI was modeled independently using a GAMM

Table 1
Sample characteristics.

A) *Demographics of study participants*

	All			Female			Male			Difference between Male and Female		
	N	Mean	SD	N	Mean	SD	N	Mean	SD	*df*	Coefficient	p-value
Age	408	14.12	1.62	177	14.03	1.57	231	14.19	1.66	406	0.12	0.30
BMIz	408	0.47	0.96	177	0.45	0.90	231	0.48	1.01	406	0.02	0.74
ICV	408	1468317	137346	177	1377606	101538	231	1537823	119612	406	113291	***<0.0001***
PDS	408	2.79	0.77	177	3.09	0.70	231	2.56	0.74	406	−0.37	***<0.0001***
SES	408	27.94	13.67	177	28.46	14.53	231	27.53	12.99	406	−0.66	0.50

B) *Associations between predictors*

	Age Coefficient			*Sex Coefficient*			*Age-by-Sex Coefficient*		
	df	*beta value*	p-value	*df*	*beta value*	p-value	*df*	*beta value*	p-value
ICV	404	692	0.84	404	113645	0.11	404	−31	1.00
BMIz	404	0.00	0.97	404	0.37	0.55	404	−0.02	0.57
SES	404	−0.11	0.80	404	1.29	0.88	404	−0.14	0.82
	PDS Coefficient			*Sex Coefficient*			*PDS-by-Sex Coefficient*		
	df	*beta value*	p-value	*df*	*beta value*	p-value	*df*	*beta value*	p-value
ICV	404	1604	0.84	404	120457	***0.0003***	404	−2327	0.83
BMIz	404	0.16	***0.02***	404	0.48	0.09	404	−0.14	0.14
SES	404	1.42	0.14	404	1.02	0.80	404	−0.41	0.76

Notes: P-values with significance level of less than 0.05 are bolded. Abbreviations: SD, standard deviation, BMIz, Body Mass Index z-score; PDS, Pubertal Development Scale; ICV, Intracranial Volume; Socioeconomic Status (SES).

(M2/M3) with fixed effects including smooth terms for age and age-by-sex (s_1 and s_2, respectively), as well as a linear term for sex, hemisphere, BMIz, ICV (for absolute volumes), SES, and a random intercept (U_i) for participant *i*:

$$M2: \ Absolute\ Probablistic\ Volume_{ij} = \beta_0 + s_1(Age_i) + \beta_1 Male_i + s_2(Age_i) \times Male_i + \beta_2 Hemisphere_{ij} + \beta_3 BMIz_i + \beta_4 ICV_i + \beta_5 SES_i + U_i + \varepsilon_{ij}$$

$$M3: \ RVF_{ij} = \beta_0 + s_1(Age_i) + \beta_1 Male_i + s_2(Age_i) \times Male_i + \beta_2 Hemisphere_{ij} + \beta_3 BMIz_i + \beta_4 SES_i + U_i + \varepsilon_{ij}$$

Where Absolute Probabilistic $Volume_{i,j}$ and $RVF_{i,j}$ were defined for each subject, *i*, in either the left or right hemisphere, *j*. Hemisphere was a nested term – for left and right – accounting for the fact that hemispheres from the same subject will be more similar than hemispheres between subjects. Each smooth term is a shrinkage version of a cubic regression spline with four equally spaced knots. ICV, SES, and BMIz are added as covariates. SES and BMI has been shown to relate to amygdala volumetric differences during adolescence (Brito and Noble, 2014; Perlaki et al., 2018). It is necessary to account for ICV, as ICV accounts for major differences in brain volumes, and thus scaling for ICV is necessary to accurately investigate valid sex differences and not solely head size differences (Pintzka et al., 2015); thus ICV was added to the absolute probabilistic volume models. For RVF, ICV was not added for our main analysis since the effect of ICV would likely not provide a significant influence given the inherent control when creating a fraction with the total amygdala; ICV was added to RVF analysis for validation and methods/results are placed in Supporting Information: Analysis of RVF covarying for ICV and Supporting Table 2.

Given that markers of pubertal development have been shown to relate to total amygdala volumes across adolescence (Goddings et al., 2014; Herting et al., 2014; Wierenga et al., 2018), we then utilized a model building strategy to determine if age, pubertal development, or their combination best predicted amygdala subregion absolute probabilistic volumes and RVFs across adolescence. Given that pubertal development follows a different age-related trajectory in males versus females and physical changes are distinct in males (e.g. facial hair, testes development) and females (e.g. breast development, menstruation) (Berenbaum et al., 2015), these analyses were performed in each sex separately. First, in each sex we examined the smooth effect of age (M4/M7). Next, we examined the smooth effect of pubertal stage (M5/M8). Lastly, we examined both the smooth effects of age and pubertal stage as well as the interaction term of age-by-pubertal stage (M6/M9), with smooths implemented by tensor product interactions, allowing for main effects and the interaction. Each model also included the fixed effects of BMIz, hemisphere, ICV (for absolute probabilistic volume models), SES, and a random intercept (U_i) for participant *i*:

$$M4: \ Absolute\ Probablistic\ Volume_{ij} = \beta_0 + s_1(Age_i) + \beta_1 Hemisphere_{ij} + \beta_2 BMIz_i + \beta_3 ICV_i + \beta_4 SES_i + U_i + \varepsilon_{ij}$$

$$M5: \ Absolute\ Probablistic\ Volume_{ij} = \beta_0 + s_1(Pubertal\ Stage_i) + \beta_1 Hemisphere_{ij} + \beta_2 BMIz_i + \beta_3 ICV_i + \beta_4 SES_i + U_i + \varepsilon_{ij}$$

$$M6: \ Absolute\ Probablistic\ Volume_{ij} = \beta_0 + s_1(Age_i) + s_2(Pubertal\ Stage_i) + s_3(Age_i,\ Pubertal\ Stage_i) + \beta_1 Hemisphere_{ij} + \beta_2 BMIz_i + \beta_3 ICV_i + \beta_4 SES_i + U_i + \varepsilon_{ij}$$

$$M7: \ RVF_{ij} = \beta_0 + s_1(Age_i) + \beta_1 Hemisphere_{ij} + \beta_2 BMIz_i + \beta_3 SES_i + U_i + \varepsilon_{ij}$$

$$M8: \ RVF_{ij} = \beta_0 + s_1(Pubertal\ Stage_i) + \beta_1 Hemisphere_{ij} + \beta_2 BMIz_i + \beta_3 SES_i + U_i + \varepsilon_{ij}$$

$$M9: \ RVF_{ij} = \beta_0 + s_1(Age_i) + s_2(Pubertal\ Stage_i) + s_3(Age_i,\ Pubertal\ Stage_i) + \beta_1 Hemisphere_{ij} + \beta_2 BMIz_i + \beta_3 SES_i + U_i + \varepsilon_{ij}$$

Akaike Information Criterion (AIC)/Bayesian Information Criterion

Table 2
Probabilistic amygdala subregions by sex.

A) Absolute probabilistic volume for each subregion (mm^3)

		LA		BLDI		BLVPL		BM		CMN		CEN		AAA		ATA		ASTA		Total	
Sex	Hemisphere	Mean	CoV (%)	Mean	CoV	Mean	CoV	Mean	CoV	Mean	CoV	Mean	CoV	Mean	CoV	Mean	CoV	Mean	CoV	Mean	CoV
Female	Left	333.78	9.73	202.35	9.71	122.42	10.69	115.67	9.74	172.01	8.96	48.19	9.94	63.08	10.23	93.11	9.93	69.83	10.47	1582.43	8.27
	Right	343.82	11.00	199.02	10.54	119.55	10.87	114.52	10.05	171.35	9.22	47.17	10.36	62.75	11.24	96.78	10.12	69.31	11.22	1593.82	9.04
Male	Left	379.49	11.45	229.99	10.21	141.37	11.74	131.25	10.12	194.88	9.44	53.37	9.74	70.69	10.25	108.77	11.25	77.05	9.82	1796.00	8.72
	Right	391.34	10.90	225.63	9.80	136.96	11.31	129.17	10.24	192.66	9.32	52.30	10.53	70.84	10.91	111.14	10.62	76.61	10.51	1804.39	8.60

B) Relative volume fraction for each subregion (to total amygdala volume)

		LA		BLDI		BLVPL		BM		CMN		CEN		AAA		ATA		ASTA	
Sex	Hemisphere	Mean	CoV (%)	Mean	CoV	Mean	CoV	Mean	CoV	Mean	CoV	Mean	CoV	Mean	CoV	Mean	CoV	Mean	CoV
Female	Left	0.21	4.92	0.13	2.78	0.08	5.45	0.07	3.80	0.11	4.65	0.03	6.88	0.04	6.07	0.06	6.69	0.04	6.80
	Right	0.22	5.32	0.12	2.85	0.07	5.24	0.07	3.98	0.11	4.55	0.03	6.33	0.04	6.64	0.06	6.80	0.04	7.15
Male	Left	0.21	5.89	0.13	3.01	0.08	6.01	0.07	4.91	0.11	5.51	0.03	7.85	0.04	6.70	0.06	7.60	0.04	7.16
	Right	0.22	5.79	0.12	2.87	0.08	6.08	0.07	4.79	0.11	4.97	0.03	7.78	0.04	6.80	0.06	7.65	0.04	7.46

Notes: Mean and coefficient of variation (CoV, mean/SD x 100 %) for each subregion's probabilistic volume in millimeters cubed (mm^3) or Relative Volume Fractions (RVF) in each brain hemisphere (right and left) for both males and females. Abbreviations: See Table 1.

(BIC) and Likelihood ratio tests ($p < 0.05$) were used to compare model fits. To reduce type I error, each set of models across the 9 ROIs were corrected for multiple comparisons using the Bonferroni correction method (Bonferroni, 1936), with p-values <0.0056 deemed significant. Effect size estimates are reported as R^2 as this summary index has been deemed most useful as an effect estimate using linear models as well as mixed effect models such as GAMM (Nakagawa and Cuthill, 2007).

3. Results

Males and females did not differ in age, BMIz, or socioeconomic status (SES) ($p > 0.05$) based on linear univariate models between the covariates and sex, though on average, males had a significantly larger ICV ($\beta = 113291$, $p < 0.0001$) compared to females and lower PDS values (β= -0.37, $p < 0.0001$) (Table 1A). M1 results are shown in Table 1B; BMIz related to pubertal status in both sexes ($\beta = 0.16$, $p < 0.02$), but associations between the variables did not significantly differ between the sexes (p's>0.05).

3.1. Amygdala subregions: age and sex effects

The mean and coefficient of variance (CoV) of the absolute probabilistic estimates and RVFs for each subregion using the CIT168 are summarized by hemisphere and sex in Fig. 3 and Table 2. From largest to smallest, absolute probabilistic estimates were on average 333−391 mm^3 for the LA (~21−22% of amygdala volume); 199-to 230 mm^3 for the BLDI (~12−13% of amygdala volume); 171−195 mm^3 for the CMN (~11 % of the amygdala volume); 119−141 mm^3 for the BLVPL (~7−8% of the amygdala volume); 114 to 131 mm^3 for the BM (~7% of the amygdala volume); 93−111 mm^3 for the ATA (~6% of the amygdala volume); 69−77 mm^3 for the ASTA (~4 % of the amygdala volume); 63−71 mm^3 for the AAA (~4% of the amygdala volume); 47−53 mm^3 for the CEN (~3% of the amygdala volume); for total amygdala volume the range was 1582−1804 mm^3.

GAMM model results examining the associations between total amygdala and each absolute probabilistic estimate (M2) or *proportion* (i.e. RVF) of the amygdala occupied by each subregion (M3) with age, sex, and age-by-sex interactions are presented in Tables 3 and 4, respectively. Age was not associated with total amygdala volume in either sex. However, a significant age-by-sex interaction was detected for both the absolute probabilistic volumes for the BLVPL (Adj $R^2 = .46$), CEN (Adj $R^2 = .45$), and ATA (Adj $R^2 = .52$) (Fig. 4), as well as the *proportion* of the amygdala occupied by these regions: BLVPL (Adj $R^2 = .13$), CEN (Adj $R^2 = .09$), ATA (Adj $R^2 = .12$) (Fig. 5). While trends were seen for the age-by-sex interaction for absolute volumes for the LA ($p = 0.095$) and ASTA ($p = 0.04$), age related differences in the *proportion* of the amygdala occupied by the LA (Adj $R^2 = .06$) and ASTA (Adj $R^2 = .06$) were significant between the sexes (Fig. 5). Specifically, the LA, CEN, and ASTA were proportionately larger (as indexed by larger RVF values) with increasing age, whereas the BLVPL and ATA were proportionately smaller with age in males. In contrast, no absolute or proportional differences were detected with age in females. A significant main effect of sex was also seen for the absolute volumes of the LA, BLDI, BM, CMN, AAA, and Total Amygdala, with males having larger volumes even after accounting for differences in ICV (Supporting Fig. 4). We also ensured findings of relative proportions were not driven by sex differences in ICV, as findings remained after including ICV in the RVF models (Supporting Information and Supporting Table 2).

3.2. Amygdala subregions: pubertal effects

GAMM model outputs for absolute probabilistic estimates (M4-M6) or *proportion* (i.e. RVF, M7-M9) for age, puberty, and age-by-puberty are presented for each sex separately. For females, no significant age, puberty, or age-by-puberty associations were seen for any of the 9 amygdala subregions (Supplemental Tables 3–4). In males, puberty and/or

Table 3
GAMM results for amygdala subregion Absolute Probabilistic Estimates associations with age, sex, and age sex interaction, controlling for hemisphere, BMI, and ICV.

LA						**CEN**					
	edf	*Ref.df*	*F*	*p-value*	Adj R squared		*edf*	*Ref.df*	*F*	*p-value*	Adj R squared
s(age)	0	3	0.00	1	0.4267	s(age)	0.00	3	0.00	0.31	0.4475
s(age*sex(male))	0.71	3	0.62	0.095		s(age*sex(male))	1.57	3	4.72	***0.0002***	
	Estimate	*SE*	*t-value*	*p-value*			*Estimate*	*SE*	*t-value*	*p-value*	
Intercept	101.6038	19.8447	5.12	***3.82E-07***		Intercept	14.0884	2.3641	5.96	***3.78E-09***	
Sex (male)	19.4378	3.8982	4.99	***7.53E-07***		Sex (male)	1.1789	0.4645	2.54	0.01	
Hemisphere (right)	11.0592	1.4848	7.45	***2.43E-13***		Hemisphere (right)	−1.0544	0.1994	−5.29	***1.60E-07***	
BMI	1.2489	1.6458	0.76	0.45		BMI	0.2950	0.1961	1.50	0.13	
ICV	1.69E-04	1.41E-05	11.96	***1.85E-30***		ICV	2.46E-05	1.68E-06	14.65	***2.91E-43***	
SES	−3.67E-02	1.16E-01	−0.32	0.75		SES	4.01E-03	1.38E-02	0.29	0.77	
BLDI						**AAA**					
	edf	*Ref.df*	*F*	*p-value*	Adj R squared		*edf*	*Ref.df*	*F*	*p-value*	Adj R squared
s(age)	0	3	0	0.56	0.4826	s(age)	0.00	3	0.00	0.32	0.3840
s(age*sex(male))	0	3	0	0.66		s(age*sex(male))	0	3	0	0.60	
	Estimate	*SE*	*t-value*	*p-value*			*Estimate*	*SE*	*t-value*	*p-value*	
Intercept	61.3836	10.5043	5.84	***7.40E-09***		Intercept	22.5640	3.3757	6.68	***4.32E-11***	
Sex (male)	1.05E+01	2.0662	5.10	***4.31E-07***		Sex (male)	3.15E+00	0.6626	4.75	***2.35E-06***	
Hemisphere (right)	−3.9146	0.7523	−5.20	***2.48E-07***		Hemisphere (right)	−0.0617	0.3411	−0.18	0.86	
BMI	−0.0742	0.8707	−0.09	0.93		BMI	0.1923	0.2798	0.69	0.49	
ICV	1.03E-04	7.46E-06	13.86	***2.47E-39***		ICV	2.93E-05	2.40E-06	12.21	***1.31E-31***	
SES	−4.01E-02	6.12E-02	−0.65	0.51		SES	−5.31E-04	1.97E-02	−0.03	0.98	
BLVPL						**ATA**					
	edf	*Ref.df*	*F*	*p-value*	Adj R squared		*edf*	*Ref.df*	*F*	*p-value*	Adj R squared
s(age)	0	3	0	0.80	0.4584	s(age)	0	3	0	0.77	0.5156
s(age*sex(male))	1.72	3	3.09	***0.0040***		s(age*sex(male))	2.31	3	12.61	***2.43E-09***	
	Estimate	*SE*	*t-value*	*p-value*			*Estimate*	*SE*	*t-value*	*p-value*	
Intercept	35.3330	7.2513	4.87	***1.33E-06***		Intercept	28.5045	5.0985	5.59	***3.09E-08***	
Sex (male)	7.8630	1.4230	5.53	***4.43E-08***		Sex (male)	7.3859	1.0006	7.38	***3.91E-13***	
Hemisphere (right)	−3.7429	0.5479	−6.83	***1.66E-11***		Hemisphere (right)	2.9350	0.4484	6.55	***1.05E-10***	
BMI	−0.4220	0.6017	−0.70	0.48		BMI	−0.5270	0.4225	−1.25	0.21	
ICV	6.45E-05	5.15E-06	12.52	***5.39E-33***		ICV	4.78E-05	3.62E-06	13.21	***3.33E-36***	
SES	−3.83E-02	4.24E-02	−0.91	0.37		SES	−2.30E-02	2.97E-02	−0.77	0.44	
BM						**ASTA**					
	edf	*Ref.df*	*F*	*p-value*	Adj R squared		*edf*	*Ref.df*	*F*	*p-value*	Adj R squared
s(age)	0	3	0	0.66	0.5124	s(age)	0	3	0	0.43	0.3838
s(age*sex(male))	0	3	0	0.67		s(age*sex(male))	0.93	3	1.18	0.04	
	Estimate	*SE*	*t-value*	*p-value*			*Estimate*	*SE*	*t-value*	*p-value*	
Intercept	27.1788	5.6527	4.81	***1.82E-06***		Intercept	22.0555	3.7145	5.94	***4.29E-09***	
Sex (male)	4.7695	1.1094	4.30	***1.92E-05***		Sex (male)	1.8162	0.7292	2.49	0.01	
Hemisphere (right)	−1.6742	0.4606	−3.63	***2.96E-04***		Hemisphere (right)	−0.4754	0.2994	−1.59	0.11	
BMI	−0.1585	0.4688	−0.34	0.74		BMI	0.3544	0.3081	1.15	0.25	
ICV	6.46E-05	4.01E-06	16.09	***9.70E-51***		ICV	3.39E-05	2.64E-06	12.86	***1.49E-34***	
SES	−4.47E-03	3.30E-02	−0.14	0.89		SES	3.09E-02	2.17E-02	1.43	0.15	
CMN						**Total**					
	edf	*Ref.df*	*F*	*p-value*	Adj R squared		*edf*	*Ref.df*	*F*	*p-value*	Adj R squared
s(age)	0	3	0	0.46	0.5070	s(age)	0	3	0	0.81	0.5790
s(age*sex(male))	0.00	3	0.00	0.40		s(age*sex(male))	0.00	3	0.00	0.91	
	Estimate	*SE*	*t-value*	*p-value*			*Estimate*	*SE*	*t-value*	*p-value*	
Intercept	55.3692	7.9193	6.99	***5.68E-12***		Intercept	476.9540	67.5772	7.06	***3.63E-12***	
Sex (male)	8.4905	1.5536	5.47	***6.16E-08***		Sex (male)	82.9533	13.2681	6.25	***6.55E-10***	
Hemisphere (right)	−1.5412	0.6473	−2.38	0.02		Hemisphere (right)	9.6899	4.6372	2.09	0.04	
BMI	3.51E-01	0.6568	0.53	0.59		BMI	1.6648	5.6050	0.30	0.77	
ICV	8.48E-05	5.62E-06	15.08	***1.75E-45***		ICV	8.05E-04	4.80E-05	16.77	***2.08E-54***	
SES	3.51E-03	4.62E-02	0.08	0.94		SES	−1.15E-01	3.94E-01	−0.29	0.77	

Notes: In each model, for the parametric terms, the estimate, standard error (SE), t-value, and p-value are shown, for the smooth terms, the estimated degree of freedom (edf), reference degree of freedom (Ref.df), F-score, and p-value are shown; the Adjusted R^2 for each model is also shown. P-values of significance level less than 0.0056 bolded. Abbreviations: See Table 1.

age-by-puberty models showed significant smooth effects for the absolute volumes and RVF estimates of the CEN, and ATA, and the RVF estimate of the BLVPL (Table 5 and Table 6). For the absolute volumes of the CEN and ATA, their volumes were found to significantly relate to pubertal status (without the inclusion of age in the model; M5 p's $<$ 0.0056) (Table 5). For the relative volumes (RVFs) of the BLVPL, CEN, and ATA, their relative volumes also significantly related to pubertal status (without the inclusion of age in the model; M8 p's $<$ 0.0056) (Table 6). Given that age and puberty are highly correlated, a model building approach allowed for us to compare if age only, puberty only, or their combination explained the most variance. For the absolute volumes of the CEN and ATA, a model comparison of age alone with age-by-puberty (M4 vs. M6) and puberty alone with age-by-puberty (M5 vs. M6) showed that the age only model did not significantly differ from the model that included both puberty and age in their interaction (M4 vs. M6: p's $\geq$ 0.05), but the model comparison between puberty alone with the interaction term showed a significant difference (M5 vs. M6: p's $<$ 0.05). This indicates that age accounts for more variance as compared to puberty. The same is true for the relative volume fractions (RVFs) of the BLVPL, CEN, and ASTA, with age alone found to be the best model. For the RVF of the ATA though, both the age and puberty alone models differed from the interaction model, but age was seen to be the driving predictor in the interaction model ($p < 0.0056$), allowing us to again conclude that age was accounting for the most variance in the RVF of the ATA. An age-by-pubertal interaction was also seen for absolute BLVPL volumes (age-by-PDS: $p = 0.02$; Adj R^2: 0.27), though it did not pass multiple comparison correction. We also confirmed adding ICV as a covariate in proportion models (i.e. RVF) lead to similar results (Supporting Tables 5 and 6).

4. Discussion

The current cross-sectional study provides the first glimpse at associations between amygdala subregion volumes and apportionment across adolescence. While previous studies have examined total amygdala volumes across childhood and adolescence (Herting et al., 2018; Wierenga et al., 2018), the current study highlights the utility of the CIT168 to define 9 amygdala subregions in a large sample of adolescents and suggests that within the amygdala distinct subregions may evolve across the adolescent period in a sex specific fashion. Using the newly derived in vivo CIT168 atlas to examine subregional volumes and proportional estimates, we found larger CEN, but smaller BLVPL and ATA subregion volumes with age in males, but not females. In addition, as a function of age-related differences in subregional volumes, the relative proportional findings suggest 17-year-old males have proportionately larger LA, CEN, and ASTA, but smaller BLVPL and ATA subregions, compared to 10-year-old males. Interestingly, the age associations in the apportionment of major subregions in males results in greater similarity of amygdala apportionment to females by age 17 years as compared to earlier on at age 10.

Although cross-sectional, our findings lend support for the hypothesis that subregions within the amygdala may have unique development patterns in males during the adolescent years. While future longitudinal MRI studies are needed to confirm potential changes in subregional volumes across development in vivo, our findings in males are supported by the recent histological study showing that postnatal neuron numbers change in distinct nuclei, including the central, lateral, and basal nuclei, from childhood to adulthood (Avino et al., 2018). In that study, however, a sex-specific effect was not examined, as the sample included a wide age range (n = 24, 2–48 years) with very few females in the neurotypical subgroup (n = 5) (Avino et al., 2018). Beyond nucleus-specific changes in neuron number, postnatal immunohistochemistry studies have also found a difference in immature and mature neuron concentrations among amygdala nuclei, including the lateral, central, basal, and paralaminar nucleus (Avino et al., 2018). A higher concentration of immature neurons has been reported in the paralaminar nucleus (part of the BLVPL subregion in the current study) as compared to other amygdala nuclei (Avino et al., 2018). Moreover, the number of immature neurons in the paralaminar nucleus decreases over time, whereas the mature neuron numbers of the surrounding regions continue to increase in childhood and adolescence. These data have led to the hypothesis that gradual maturation and migration of paralaminar immature neurons may contribute to the mature neuron number within the paralaminar, and/or be the source of increases in neuron number seen in other nuclei over development (deCampo and Fudge, 2012; Avino et al., 2018). If this hypothesis proves to be correct, migration and maturation of immature neurons may contribute to the size as well as the re-configuration and/or refinement of the amygdala subregions and their subsequent connectivity with the cerebral cortex across adolescence. While MRI cannot assess neuron number, more research is needed to determine if age associations with the absolute volumes of the BLVPL, CEN, and ATA as well as age related differences in the relative proportion of these amygdala subregions, along with the LA and ASTA, in males may be suggestive of distinct nuclei maturation and migration patterns in amygdala development. Combining postmortem histology and MRI segmentation approaches in developing samples is necessary to further decipher if these age and sex-specific patterns occur across development.

Furthermore, cytoarchitectural findings suggest the BLVPL subregion of the amygdala receives afferents from both the lateral nucleus (LA) and the hippocampus (Pitkanen and Amaral, 1998). Efferents of the medial paralaminar nucleus gradually merge with the periamygdaloid cortex, corresponding to the amygdaloid transition areas (ATA) in this study, which in turn projects to the hippocampus. Moreover, the lateral nucleus (LA) receives sensory information, allowing the basolateral complex to process the information, and then send this information out of the amygdala via the central nucleus (CEN) (McDonald and Jackson, 1987; Sah et al., 2003). The CIT168 ATA region encapsulates the periamygdaloid cortex, as well as these amygdalocortical and amygdolohippocampal transition areas. Hippocampal input to the amygdala is important for contextual fear learning (Phillips and LeDoux, 1992), and given the convergence between sensory input from the LA, as well as bidirectional connectivity with the hippocampus, it has been proposed that the paralaminar and periamygdaloid cortex of the amygdala may be involved in contextual learning (deCampo and Fudge, 2013). It remains to be elucidated how larger LA, ASTA, and CEN, but smaller BLVPL and ATA apportionment in males may map onto function. However, amygdala nuclei size and relative composition may be an additional MRI feature to explore in hopes of clarifying our understanding of amygdala structural and functional development. It may also prove useful in studying known sex differences in emotion-related behavior, brain function, and prevalence in mental health disorders that typically emerge during this time. For example, meta-analysis of 166 studies found a small, yet consistent, sex difference in positive and negative emotional expression that begins to diverge in the beginning of childhood and into adolescence (Chaplin and Aldao, 2013). Similarly, fMRI studies have reported greater brain activity in cortical regions, including visual and parietal regions, in male versus female adolescents during emotional functional MRI tasks (Cservenka et al., 2015). Resting-state fMRI studies implementing ex vivo atlases to define basolateral, superficial, and centromedial subregions, have also found age and sex-specific differences in amygdala functional connectivity patterns. Age and region-specific patterns have been seen, with an age-related increases in amygdala to medial prefrontal cortex (mPFC) functional connectivity in children and adolescents (Gabard-Durnam et al., 2014; Alarcon et al., 2015). These studies also found an age-related decrease in functional connectivity between the amygdala and the insula and superior temporal sulcus (STS) (Gabard-Durnam et al., 2014), the parahippocampal gyrus and posterior cingulate regions (Gabard-Durnam et al., 2014), and the parieto-occipital cortices (Alarcon et al., 2015). Across the age ranges included in Gabard-Durnam et al., 2014, an apparent inflection point at age 10 from zero to positive or negative coupling was seen for these patterns of amygdala-cortical functional connectivity across both

Table 4
GAMM results for amygdala subregion Relative Volume Fraction (RVF) associations with age, sex, and age sex interaction, controlling for hemisphere and BMI.

LA

	edf	*Ref.df*	*F*	*p-value*	Adj R squared
s(age)	0	3	0.00	0.83	0.0594
s(age*sex(male))	1.26	3	2.69	***0.00355***	
	Estimate	*SE*	*t-value*	*p-value*	
Intercept	0.2108	0.0013	158.16	***0.00E+00***	
Sex (male)	0.0006	0.0010	0.55	0.58	
Hemisphere (right)	0.0052	0.0006	8.83	***6.40E-18***	
BMI	0.0006	0.0005	1.16	0.25	
SES	−1.45E-05	3.69E-05	−0.39	0.69	

CEN

	edf	*Ref.df*	*F*	*p-value*	Adj R squared
s(age)	0.65	3	0.45	0.13	0.0939
s(age*sex(male))	2.22	3	3.82	***0.00090***	
	Estimate	*SE*	*t-value*	*p-value*	
Intercept	0.0303	0.0002	128.16	***0.00E+00***	
Sex (male)	−0.0007	0.0002	−3.70	***2.26E-04***	
Hemisphere (right)	−0.0008	0.0001	−7.07	***3.28E-12***	
BMI	0.0001	0.0001	1.39	0.16	
SES	4.50E-06	6.52E-06	0.69	0.49	

BLDI

	edf	*Ref.df*	*F*	*p-value*	Adj R squared
s(age)	0	3	0	0.38	0.1473
s(age*sex(male))	0	3	0	0.21	
	Estimate	*SE*	*t-value*	*p-value*	
Intercept	0.1283	0.0004	309.45	***0.00E+00***	
Sex (male)	1.93E-04	0.0003	0.61	0.54	
Hemisphere (right)	−0.0030	0.0002	−16.60	***1.70E-53***	
BMI	−0.0002	0.0002	−1.13	0.26	
SES	−1.53E-05	1.15E-05	−1.33	0.18	

AAA

	edf	*Ref.df*	*F*	*p-value*	Adj R squared
s(age)	0.15	3	0.06	0.28	0.0028
s(age*sex(male))	0	3	0	0.64	
	Estimate	*SE*	*t-value*	*p-value*	
Intercept	0.0396	0.0003	141.51	***0.00E+00***	
Sex (male)	−2.92E-04	0.0002	−1.39	0.16	
Hemisphere (right)	−0.0003	0.0002	−1.91	0.06	
BMI	0.0001	0.0001	0.70	0.48	
SES	3.08E-06	7.66E-06	0.40	0.69	

BLVPL

	edf	*Ref.df*	*F*	*p-value*	Adj R squared
s(age)	0	3	0	0.84	0.1299
s(age*sex(male))	2.08	3	7.92	***2.24E-06***	
	Estimate	*SE*	*t-value*	*p-value*	
Intercept	0.0781	0.0005	162.36	***0.00E+00***	
Sex (male)	0.0011	0.0004	3.04	***2.40E-03***	
Hemisphere (right)	−0.0026	0.0002	−11.09	***1.01E-26***	
BMI	−0.0003	0.0002	−1.48	0.14	
SES	−1.88E-05	1.33E-05	−1.42	0.16	

ATA

	edf	*Ref.df*	*F*	*p-value*	Adj R squared
s(age)	0	3	0	0.56	0.1206
s(age*sex(male))	2.27	3	15.78	***1.23E-11***	
	Estimate	*SE*	*t-value*	*p-value*	
Intercept	0.0596	0.0005	125.32	***0.00E+00***	
Sex (male)	0.0013	0.0004	3.67	***2.61E-04***	
Hemisphere (right)	0.0014	0.0002	6.52	***1.25E-10***	
BMI	−0.0003	0.0002	−1.73	0.08	
SES	−1.02E-05	1.31E-05	−0.77	0.44	

BM

	edf	*Ref.df*	*F*	*p-value*	Adj R squared
s(age)	0	3	0	0.74	0.0433
s(age*sex(male))	0	3	0	0.47	
	Estimate	*SE*	*t-value*	*p-value*	
Intercept	0.0731	0.0004	204.29	***0.00E+00***	
Sex (male)	−0.0001	0.0003	−0.44	0.66	
Hemisphere (right)	−0.0014	0.0002	−7.93	***7.28E-15***	
BMI	−0.0002	0.0001	−1.47	0.14	
SES	3.80E-06	9.85E-06	0.39	0.70	

ASTA

	edf	*Ref.df*	*F*	*p-value*	Adj R squared
s(age)	0	3	0	0.31	0.0563
s(age*sex(male))	1.33	3	2.54	***0.00557***	
	Estimate	*SE*	*t-value*	*p-value*	
Intercept	0.0434	0.0003	126.29	***0.00E+00***	
Sex (male)	−0.0011	0.0003	−4.17	***3.36E-05***	
Hemisphere (right)	−0.0005	0.0002	−3.40	***6.99E-04***	
BMI	0.0002	0.0001	1.17	0.24	
SES	2.07E-05	9.50E-06	2.18	0.03	

CMN

	edf	*Ref.df*	*F*	*p-value*	Adj R squared
s(age)	0	3	0	0.59	0.0177
s(age*sex(male))	0.15	3	0.06	0.28	
	Estimate	*SE*	*t-value*	*p-value*	
Intercept	0.1086	0.0006	177.73	***0.00E+00***	
Sex (male)	−0.0005	0.0005	−0.98	0.33	
Hemisphere (right)	−0.0015	0.0003	−5.59	***3.17E-08***	
BMI	9.39E-05	0.0002	0.39	0.70	
SES	1.15E-05	1.69E-05	0.68	0.50	

Notes: In each model, for the parametric terms, the estimate, standard error (SE), t-value, and p-value are shown, for the smooth terms, the estimated degree of freedom (edf), reference degree of freedom (Ref.df), F-score, and p-value are shown; the Adjusted R^2 for each model is also shown. P-values of significance level less than 0.0056 bolded. Abbreviations: See Table 1.

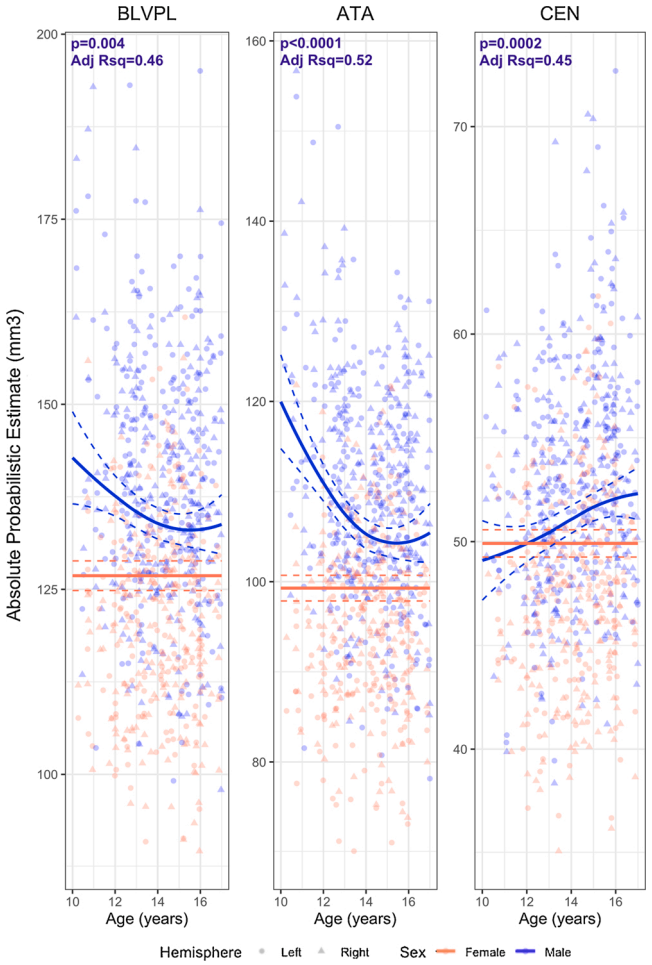

Fig. 4. Sex differences in age associations with Absolute Probabilistic Estimate of the amygdala subregions. A) Basolateral ventral and paralaminar subdivision (BLVPL) and B) Central (CEN) and C) Amygdala transition area (ATA). Absolute Probabilistic Estimate plotted by age and sex (collapsed across hemispheres); solid lines reflect GAMM predicted fit estimates and dashed lines reflect 95 % confidence intervals; p-value represents the smooth age-by-sex interaction term.

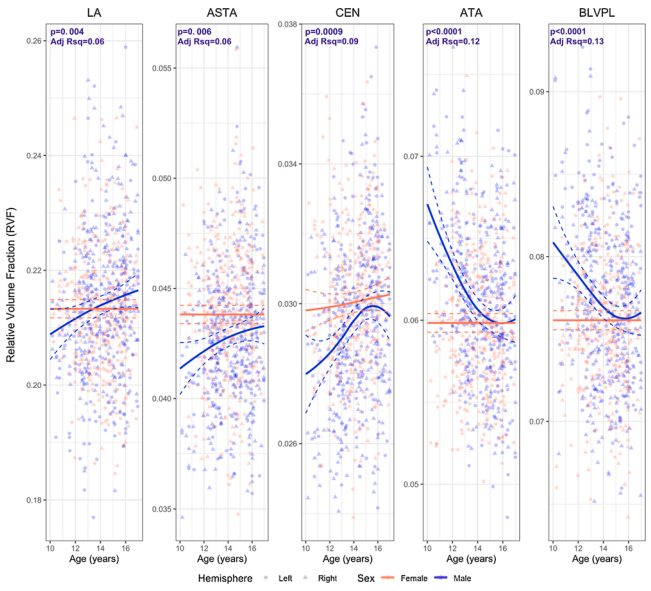

Fig. 5. Sex differences in age associations with RVF of the amygdala subregions. A) Lateral nucleus (LA), B) Basolateral ventral and paralaminar subdivision (BLVPL) and C) Central (CEN) D) Amygdala transition area (ATA) and E) Amygdalostriatal transition area (ASTA). Relative Volume France (RVF) plotted by age and sex (collapsed across hemispheres); solid lines reflect GAMM predicted fit estimates and dashed lines reflect 95 % confidence intervals; p-value represents the smooth age-by-sex interaction term.

sexes (i.e. no age-by-sex or sex effects seen for N = 58) (Gabard-Durnam et al., 2014), whereas in Alarcon et al., 2015, sex differences were seen in the resting-state patterns of the superficial amygdala (which incorporates the AAA, ATA, CMN) and basolateral amygdala (which incorporates the LA, BLDI, BLVPL, BM) (N = 122) (Alarcon et al., 2015). While more research is needed, it is feasible that these age and sex related patterns of functional connectivity may be linked to the current structural findings. For example, increases in the amygdala-to-mPFC could be attributed to the LA increases and modulated by the BLVPL decreases, given that animal studies have found that the basolateral nucleus (which merges the LA, BM, BLDI, BLVPL) has the most substantial connections to the mPFC (Reppucci and Petrovich, 2016). Moreover, the decrease in amygdala-to-parahippocampal gyrus/posterior cingulate functional connectivity may be related to age-related patterns of BLVPL, ATA, and ASTA volumes, since retrograde primate studies have shown hippocampal connections target the ventromedial amygdala (Fudge et al., 2012). Similarly, decreases in amygdala-to-insula/STS and amygdala-to-parieto-orbital functional connectivity may be attributed to its connections with the LA and CEN (Herzog and Van Hoesen, 1976; Sah et al., 2003). The current sex differences in age-related volumetric patterns in the LA and BLVPL are also congruent with previous findings that basolateral amygdala (which incorporate the LA, BLDI, BLVPL, BM) connectivity patterns were more mature in male adolescents (Alarcon et al., 2015). Future studies are warranted to determine if the absolute and/or relative differences in the volumes of primary input (LA) and output (CEN) subregions, as well as subregions involved in contextual and emotional learning (BLVPL, ATA) in males, may relate to differences in emotional expression, greater cortical activation to emotional stimuli and/or stronger basolateral functional connectivity in males versus females during adolescence. Beyond the possible functional implications of nuclei apportionment, implementation of the CIT168 atlas to construct ROIs for other MRI modalities, including resting-state fMRI, task-based fMRI, and diffusion, may also assist in gaining greater specificity of how different amygdala nuclei functionally and structurally develop.

While this is the first study to examine amygdala subregional volume composition in adolescents, the current study has both strengths and limitations. Other amygdala segmentation approaches are derived from post-mortem samples that are largely based on smaller samples of older male brains (Amunts et al., 2005; Saygin et al., 2017), which not only fail to capture possible developmental changes but may also be confounded by factors that influence tissue quality (Stan et al., 2006). The CIT168 atlas mitigates some of these concerns by using the high-resolution (700 μm) in vivo Human Connectome Project data from young adults (ages 22–35 years) and by using probabilistic delineations to encode partial volume uncertainty in amygdala subregion boundaries. While the CIT168 probabilistic amygdala atlas has several advantages over other currently available approaches, challenges still exist when registering templates derived from in vivo adult human data to anatomic data acquired in developing human children on different scanners, at different field strengths, and with differing imaging parameters. Amygdala nuclei remain extremely difficult to discern by eye in typical 3 T whole brain T1- or T2-weighted images, including those in the current study. While we have used conservative exclusion criteria for minimum CNR to improve the robustness of our volume estimates,

Table 5
GAMM amygdala subregion Absolute Probabilistic Estimate results for age, pubertal status, and age-by-pubertal status interaction for males.

MALES

Total	**Smooth Terms**						**Model Fit**					
	Terms	**edf**	**Ref.df**	**F**	**p-value**	**R2**	**df**	**AIC**	**BIC**	**logLik**	**Test**	**L.Ratio**	**p-value**
M4	s(age)	0.03	3.00	0.00	0.9176	0.3544	8	5615.69	5648.70	−2799.84	M4 vs. M6	1.83	0.7676
M5	s(pds)	0.02	3.00	0.00	1.0000	0.3544	8	5615.69	5648.70	−2799.84	M5 vs. M6	1.83	0.7678
M6	ti(age)	0.00	3.00	0.00	0.8394	0.3572	12	5621.86	5671.38	−2798.93			
	ti(pds)	0.00	3.00	0.00	0.6553								
	ti(age, pds)	1.02	1.02	1.73	0.1847								
LA	**Smooth Terms**						**Model Fit**					
	Terms	**edf**	**Ref.df**	**F**	**p-value**	**R2**	**df**	**AIC**	**BIC**	**logLik**	**Test**	**L.Ratio**	**p-value**
M4	s(age)	0.62	3.00	0.44	0.1398	0.2106	8	4539.26	4572.27	−2261.63	M4 vs. M6	0.11	0.9986
M5	s(pds)	0.43	3.00	0.24	0.1958	0.2088	8	4539.52	4572.54	−2261.76	M5 vs. M6	0.37	0.9845
M6	ti(age)	0.58	3.00	0.47	0.1141	0.2098	12	4547.15	4596.67	−2261.57			
	ti(pds)	0.01	3.00	0.00	0.3013								
	ti(age, pds)	1.04	1.04	0.13	0.7324								
BLDI	**Smooth Terms**						**Model Fit**					
	Terms	**edf**	**Ref.df**	**F**	**p-value**	**R2**	**df**	**AIC**	**BIC**	**logLik**	**Test**	**L.Ratio**	**p-value**
M4	s(age)	0.02	3.00	0.00	0.6726	0.2587	8	3930.65	3963.67	−1957.33	M4 vs. M6	1.96	0.7440
M5	s(pds)	0.03	3.00	0.00	0.5643	0.2587	8	3930.65	3963.67	−1957.33	M5 vs. M6	1.95	0.7441
M6	ti(age)	0.00	3.00	0.00	1.0000	0.2622	12	3936.70	3986.22	−1956.35			
	ti(pds)	0.00	3.00	0.00	0.8437								
	ti(age, pds)	1.02	1.02	1.86	0.1691								
BLVPL	**Smooth Terms**						**Model Fit**					
	Terms	**edf**	**Ref.df**	**F**	**p-value**	**R2**	**df**	**AIC**	**BIC**	**logLik**	**Test**	**L.Ratio**	**p-value**
M4	s(age)	1.64	3.00	2.55	0.0098	0.2559	8	3621.25	3654.27	−1802.63	M4 vs. M6	4.79	0.3095
M5	s(pds)	0.74	3.00	0.69	0.0877	0.2405	8	3623.92	3656.94	−1803.96	M5 vs. M6	7.46	0.1136
M6	ti(age)	0.06	3.00	0.03	0.2222	0.2697	12	3624.46	3673.99	−1800.23			
	ti(pds)	0.02	3.00	0.00	0.3375								
	ti(age, pds)	3.31	3.31	3.15	0.0207								
BM	**Smooth Terms**						**Model Fit**					
	Terms	**edf**	**Ref.df**	**F**	**p-value**	**R2**	**df**	**AIC**	**BIC**	**logLik**	**Test**	**L.Ratio**	**p-value**
M4	s(age)	0.02	3.00	0.00	0.6703	0.3370	8	3417.37	3450.39	−1700.69	M4 vs. M6	1.19	0.8792
M5	s(pds)	0.02	3.00	0.00	0.6011	0.3370	8	3417.37	3450.39	−1700.69	M5 vs. M6	1.19	0.8792
M6	ti(age)	0.00	3.00	0.00	0.8597	0.3382	12	3424.18	3473.70	−1700.09			
	ti(pds)	0.00	3.00	0.00	0.8333								
	ti(age, pds)	1.01	1.01	1.15	0.2816								
CMN	**Smooth Terms**						**Model Fit**					
	Terms	**edf**	**Ref.df**	**F**	**p-value**	**R2**	**df**	**AIC**	**BIC**	**logLik**	**Test**	**L.Ratio**	**p-value**
M4	s(age)	0.06	3.00	0.01	0.4113	0.3280	8	3709.99	3743.00	−1846.99	M4 vs. M6	2.97	0.5636
M5	s(pds)	0.02	3.00	0.00	0.8086	0.3279	8	3709.98	3743.00	−1846.99	M5 vs. M6	2.96	0.5639
M6	ti(age)	0.00	3.00	0.00	0.6853	0.3331	12	3715.02	3764.54	−1845.51			
	ti(pds)	0.00	3.00	0.00	0.7963								
	ti(age, pds)	1.01	1.01	2.84	0.0893								
CEN	**Smooth Terms**						**Model Fit**					
	Terms	**edf**	**Ref.df**	**F**	**p-value**	**R2**	**df**	**AIC**	**BIC**	**logLik**	**Test**	**L.Ratio**	**p-value**
M4	s(age)	1.54	3.00	4.38	***0.0003***	0.3246	8	2597.87	2630.88	−1290.93	M4 vs. M6	0.74	0.9466
M5	s(pds)	1.07	3.00	2.55	***0.0040***	0.3121	8	2601.82	2634.83	−1292.91	M5 vs. M6	4.68	0.3212
M6	ti(age)	2.12	3.00	5.82	***0.0001***	0.3337	12	2605.13	2654.65	−1290.57			
	ti(pds)	0.00	3.00	0.00	0.8718								
	ti(age, pds)	1.01	1.01	1.24	0.2647								
AAA	**Smooth Terms**						**Model Fit**					
	Terms	**edf**	**Ref.df**	**F**	**p-value**	**R2**	**df**	**AIC**	**BIC**	**logLik**	**Test**	**L.Ratio**	**p-value**
M4	s(age)	0.01	3.00	0.00	0.5225	0.2070	8	3050.85	3083.87	−1517.43	M4 vs. M6	1.61	0.8061
M5	s(pds)	0.00	3.00	0.00	1.0000	0.2070	8	3050.85	3083.87	−1517.43	M5 vs. M6	1.61	0.8063
M6	ti(age)	0.00	3.00	0.00	1.0000	0.2138	12	3057.24	3106.76	−1516.62			
	ti(pds)	0.00	3.00	0.00	0.7833								
	ti(age, pds)	2.37	2.37	2.15	0.2846								
ATA	**Smooth Terms**						**Model Fit**					
	Terms	**edf**	**Ref.df**	**F**	**p-value**	**R2**	**df**	**AIC**	**BIC**	**logLik**	**Test**	**L.Ratio**	**p-value**
M4	s(age)	2.32	3.00	11.74	***1.57E-08***	0.3339	8	3347.79	3380.80	−1665.89	M4 vs. M6	1.13	0.8892
M5	s(pds)	1.26	3.00	3.70	***0.0008***	0.2828	8	3365.61	3398.62	−1674.80	M5 vs. M6	18.95	***0.0008***
M6	ti(age)	1.46	3.00	4.84	***0.0001***	0.3294	12	3354.66	3404.18	−1665.33			
	ti(pds)	0.01	3.00	0.00	0.4392								
	ti(age, pds)	1.13	1.13	2.52	0.0904								

(*continued on next page*)

Table 5 (*continued*)

MALES												
ASTA	**Smooth Terms**					**Model Fit**						
	Terms	**edf**	**Ref.df**	**F**	**p-value**	**R2**	**df**	**AIC**	**BIC**	**logLik**	**Test**	**L.Ratio**	**p-value**
M4	s(age)	0.92	3.00	1.15	0.0401	0.2312	8	2989.47	3022.48	−1486.73	M4 vs. M6	0.01	1.0000
M5	s(pds)	0.62	3.00	0.47	0.1292	0.2255	8	2990.84	3023.85	−1487.42	M5 vs. M6	1.36	0.8518
M6	ti(age)	0.80	3.00	1.03	0.0425	0.2295	12	2997.48	3047.00	−1486.74			
	ti(pds)	0.01	3.00	0.00	0.6686								
	ti(age, pds)	1.02	1.02	0.01	0.9082								

Notes: In each model, the smooth terms, the estimated degree of freedom (edf), reference degree of freedom (Ref.df), F-score, p-value, and Adjusted R^2 for each model is shown; p-value < 0.0056 bolded (Bonferroni corrected). Between model comparisons include the df, AIC, BIC, log-likelihood ratio (L Ratio) and p-values < 0.05 bolded.

Table 6
GAMM amygdala subregion Relative Volume Fraction (RVF) results for age, pubertal status, and age-by-pubertal status interaction for males.

MALES												
LA	**Smooth Terms**					**Model Fit**						
	Terms	**edf**	**Ref.df**	**F**	**p-value**	**R2**	**df**	**AIC**	**BIC**	**logLik**	**Test**	**L.Ratio**	**p-value**
M7	s(age)	1.22	3.00	2.32	0.0069	0.0745	7	−2779.68	−2750.79	1396.84	M7 vs. M9	0.29	0.9903
M8	s(pds)	0.90	3.00	1.30	0.0300	0.0650	7	−2777.51	−2748.62	1395.76	M8 vs. M9	2.46	0.6514
M9	ti(age)	0.95	3.00	1.77	0.0132	0.0722	11	−2771.97	−2726.58	1396.99			
	ti(pds)	0.00	3.00	0.00	0.6037								
	ti(age, pds)	1.00	1.00	0.34	0.5605								
BLDI	**Smooth Terms**					**Model Fit**						
	Terms	**edf**	**Ref.df**	**F**	**p-value**	**R2**	**df**	**AIC**	**BIC**	**logLik**	**Test**	**L.Ratio**	**p-value**
M7	s(age)	0.49	3.00	0.25	0.2163	0.1388	7	−3876.94	−3848.05	1945.47	M7 vs. M9	1.66	0.7988
M8	s(pds)	0.80	3.00	0.95	0.0526	0.1451	7	−3878.31	−3849.42	1946.15	M8 vs. M9	0.28	0.9909
M9	ti(age)	0.00	3.00	0.00	0.8181	0.1436	11	−3870.59	−3825.20	1946.30			
	ti(pds)	0.69	3.00	0.71	0.0757								
	ti(age, pds)	1.01	1.01	0.29	0.5876								
BLVPL	**Smooth Terms**					**Model Fit**						
	Terms	**edf**	**Ref.df**	**F**	**p-value**	**R2**	**df**	**AIC**	**BIC**	**logLik**	**Test**	**L.Ratio**	**p-value**
M7	s(age)	2.32	3.00	10.61	***8.00E-08***	0.1392	7	−3629.03	−3600.14	1821.51	M7 vs. M9	3.14	0.5345
M8	s(pds)	1.11	3.00	2.95	***0.0021***	0.1062	7	−3677.58	−3648.69	1845.79	M8 vs. M9	45.41	***3.26E-09***
M9	ti(age)	1.98	3.00	6.29	***7.09E-06***	0.1718	11	−3624.17	−3578.77	1823.08			
	ti(pds)	0.01	3.00	0.00	0.2791								
	ti(age, pds)	5.63	5.63	2.39	0.1672								
BM	**Smooth Terms**					**Model Fit**						
	Terms	**edf**	**Ref.df**	**F**	**p-value**	**R2**	**df**	**AIC**	**BIC**	**logLik**	**Test**	**L.Ratio**	**p-value**
M7	s(age)	0.00	3.00	0.00	0.4152	0.0394	7	−3863.77	−3834.89	1938.89	M7 vs. M9	0.95	0.9175
M8	s(pds)	0.30	3.00	0.13	0.2510	0.0402	7	−3863.82	−3834.93	1938.91	M8 vs. M9	0.90	0.9242
M9	ti(age)	0.00	3.00	0.00	0.6623	0.0446	11	−3856.72	−3811.33	1939.36			
	ti(pds)	0.01	3.00	0.00	0.4209								
	ti(age, pds)	2.40	2.40	0.71	0.4121								
CMN	**Smooth Terms**					**Model Fit**						
	Terms	**edf**	**Ref.df**	**F**	**p-value**	**R2**	**df**	**AIC**	**BIC**	**logLik**	**Test**	**L.Ratio**	**p-value**
M7	s(age)	0.09	3.00	0.03	0.3300	0.0208	7	−3502.36	−3473.47	1758.18	M7 vs. M9	0.29	0.9902
M8	s(pds)	0.02	3.00	0.00	0.7752	0.0204	7	−3502.35	−3473.46	1758.18	M8 vs. M9	0.30	0.9896
M9	ti(age)	0.00	3.00	0.00	0.3768	0.0195	11	−3494.65	−3449.26	1758.33			
	ti(pds)	0.00	3.00	0.00	0.9123								
	ti(age, pds)	1.05	1.05	0.26	0.6056								
CEN	**Smooth Terms**					**Model Fit**						
	Terms	**edf**	**Ref.df**	**F**	**p-value**	**R2**	**df**	**AIC**	**BIC**	**logLik**	**Test**	**L.Ratio**	**p-value**
M7	s(age)	2.53	3.00	11.10	***8.04E-08***	0.0904	7	−4274.82	−4245.93	2144.41	M7 vs. M9	0.65	0.9573
M8	s(pds)	1.10	3.00	2.94	***0.0020***	0.0526	7	−4323.70	−4294.82	2168.85	M8 vs. M9	48.23	***8.44E-10***
M9	ti(age)	2.51	3.00	10.09	***1.72E-07***	0.0920	11	−4267.47	−4222.08	2144.74			
	ti(pds)	0.00	3.00	0.00	0.7837								
	ti(age, pds)	1.10	1.10	0.70	0.4312								
AAA	**Smooth Terms**					**Model Fit**						
	Terms	**edf**	**Ref.df**	**F**	**p-value**	**R2**	**df**	**AIC**	**BIC**	**logLik**	**Test**	**L.Ratio**	**p-value**
M7	s(age)	0.01	3.00	0.00	0.5058	−0.0058	7	−4121.01	−4092.13	2067.51	M7 vs. M9	1.46	0.8331
M8	s(pds)	0.01	3.00	0.00	0.9963	−0.0058	7	−4121.01	−4092.12	2067.50	M8 vs. M9	1.47	0.8321
M9	ti(age)	0.02	3.00	0.00	0.4720	0.0077	11	−4114.48	−4069.08	2068.24			
	ti(pds)	0.01	3.00	0.00	0.9471								
	ti(age, pds)	3.56	3.56	1.65	0.2284								

(*continued on next page*)

Table 6 (*continued*)

MALES													
ATA	**Smooth Terms**						**Model Fit**						
	Terms	**edf**	**Ref.df**	**F**	**p-value**	**R2**	**df**	**AIC**	**BIC**	**logLik**	**Test**	**L.Ratio**	**p-value**
M7	s(age)	2.47	3.00	22.82	***1.80E-15***	0.1556	7	−3672.81	−3643.93	1843.41	M7 vs. M9	59.58	***3.56E-12***
M8	s(pds)	1.31	3.00	5.59	***3.35E-05***	0.0819	7	−3711.02	−3682.13	1862.51	M8 vs. M9	21.38	***0.0003***
M9	ti(age)	2.16	3.00	10.72	***2.36E-08***	0.1546	11	−3724.39	−3679.00	1873.20			
	ti(pds)	0.00	3.00	0.00	0.5055								
	ti(age, pds)	1.01	1.01	0.03	0.8626								
ASTA	**Smooth Terms**						**Model Fit**						
	Terms	**edf**	**Ref.df**	**F**	**p-value**	**R2**	**df**	**AIC**	**BIC**	**logLik**	**Test**	**L.Ratio**	**p-value**
M7	s(age)	1.62	3.00	4.10	***0.0006***	0.0328	7	−3980.89	−3952.00	1997.44	M7 vs. M9	2.69	0.6107
M8	s(pds)	0.76	3.00	0.80	0.0695	0.0153	7	−4034.94	−4006.05	2024.47	M8 vs. M9	51.36	***1.88E-10***
M9	ti(age)	0.75	3.00	0.91	0.0427	0.0409	11	−3975.58	−3930.18	1998.79			
	ti(pds)	0.02	3.00	0.00	0.3549								
	ti(age, pds)	3.02	3.02	2.08	0.0904								

Notes: In each model, the smooth terms, the estimated degree of freedom (edf), reference degree of freedom (Ref.df), F-score, p-value, and Adjusted R^2 for each model is shown; p-value < 0.0056 bolded (Bonferroni corrected). Between model comparisons include the df, AIC, BIC, log-likelihood ratio (L Ratio) and p-values < 0.05 bolded.

replication studies at higher field strengths (e.g. 7 T) with better individual-level amygdala CNR would be extremely valuable. Though, it is interesting to note, that the size of the subregion did not seem to affect the results, as the largest region (LA) and the smallest (CEN) both showed associations. A few additional limitations should also be noted. First, the current study is cross-sectional and therefore cannot attest to the development of the amygdala over time in the same individuals. Future longitudinal studies are necessary and warranted to further elucidate potential maturational patterns of amygdala subregion volumes and apportionment in each sex and as individuals undergo pubertal maturation. From this cross-sectional analysis, our hypothesis that pubertal development would relate to amygdala composition during adolescence was not well supported. While physical characteristics of pubertal maturation did relate to BLVPL, CEN, and ATA, our current results suggest that age alone best accounts for individual differences in amygdala nuclei volume composition in males. Moreover, neither age nor pubertal status related to any of the nuclei examined in females. It is possible the lack of associations is due to our study sample. Pubertal development scores were on average lower in males than females in our sample (Table 1); therefore, there were fewer females that fell within the pre-pubertal and early pubertal range as compared to males in this age range of 10–17 years. While this is to be expected given the known sex difference in pubertal onset, with girls showing physical signs of maturation ~1−2 years prior to males (Dorn, 2006), more research is needed in younger females in order to assess if similar patterns of amygdala maturation do occur at slightly younger ages in females. Furthermore, as a focus of future research, it would also be helpful to utilize other markers that may be more accurate for capturing both puberty in children, such as pubertal hormone levels.

5. Conclusion

To summarize, we show the adolescent amygdala can be segmented into 9 subregions using the newly developed CIT168 atlas and that the relative composition of these amygdala subregions may continue to restructure in a sex-specific fashion during the adolescent window of development. By using this approach in conjunction with considering how the amygdala nuclei composition may continue to develop, future studies may be able to further explore how the amygdaloid complex may interact with distinct cortical regions, such as the prefrontal cortex, in order to modulate each other's development and social and emotional behaviors that continue to mature during this critical period in development (Andersen and Teicher, 2008; Tottenham and Gabard-Durnam, 2017). Our approach provides a first step towards a more rigorous exploration of functional and structural connectivity development within the heterogeneous amygdala complex across adolescence.

Declaration of Competing Interest

The authors declare that they have no known competing financial interests or personal relationships that could have appeared to influence the work reported in this paper.

Acknowledgements

The research above was supported by the following grants, R01 AA017664 (PI: Nagel), R21 MH099618 (PI: Nagel), R03 HD090308 (PI: Herting), K01 MH108761 (PI: Herting), and NIMH P50 MH094258 #8198 (PI: Tyszka). We also thank the families who contributed their time and participated in the above study.

Appendix A. Supplementary data

Supplementary material related to this article can be found, in the online version, at doi:https://doi.org/10.1016/j.dcn.2020.100883.

References

Alarcon, G., Cservenka, A., Rudolph, M.D., Fair, D.A., Nagel, B.J., 2015. Developmental sex differences in resting state functional connectivity of amygdala sub-regions. Neuroimage 115, 235–244.
Amaral, D.G., Price, J.L., 1984. Amygdalo-cortical projections in the monkey (Macaca fascicularis). J. Comp. Neurol. 230 (4), 465–496.
Amunts, K., Kedo, O., Kindler, M., Pieperhoff, P., Mohlberg, H., Shah, N.J., Habel, U., Schneider, F., Zilles, K., 2005. Cytoarchitectonic mapping of the human amygdala, hippocampal region and entorhinal cortex: intersubject variability and probability maps. Anat. Embryol. (Berl.) 210 (5–6), 343–352.
Andersen, S.L., Teicher, M.H., 2008. Stress, sensitive periods and maturational events in adolescent depression. Trends Neurosci. 31 (4), 183–191.
Avants, B., Anderson, C., Grossman, M., Gee, J.C., 2007. Spatiotemporal normalization for longitudinal analysis of gray matter atrophy in frontotemporal dementia. Med. Image Comput. Comput. Assist. Interv. 10 (Pt 2), 303–310.
Avants, B.B., Tustison, N.J., Song, G., Cook, P.A., Klein, A., Gee, J.C., 2011. A reproducible evaluation of ANTs similarity metric performance in brain image registration. Neuroimage 54 (3), 2033–2044.

Avino, T.A., Barger, N., Vargas, M.V., Carlson, E.L., Amaral, D.G., Bauman, M.D., Schumann, C.M., 2018. Neuron numbers increase in the human amygdala from birth to adulthood, but not in autism. Proc. Natl. Acad. Sci. U. S. A. 115 (14), 3710–3715.
Backhausen, L.L., Herting, M.M., Buse, J., Roessner, V., Smolka, M.N., Vetter, N.C., 2016. Quality control of structural MRI images applied using FreeSurfer-A hands-on workflow to rate motion artifacts. Front. Neurosci. 10, 558.
Barbas, H., De Olmos, J., 1990. Projections from the amygdala to basoventral and mediodorsal prefrontal regions in the rhesus monkey. J. Comp. Neurol. 300 (4), 549–571.
Baxter, M.G., Murray, E.A., 2002. The amygdala and reward. Nat. Rev. Neurosci. 3 (7), 563–573.
Berenbaum, S.A., Beltz, A.M., Corley, R., 2015. The importance of puberty for adolescent development: conceptualization and measurement. Adv. Child Dev. Behav. 48, 53–92.
Bernier, P.J., Bedard, A., Vinet, J., Levesque, M., Parent, A., 2002. Newly generated neurons in the amygdala and adjoining cortex of adult primates. Proc. Natl. Acad. Sci. U. S. A. 99 (17), 11464–11469.
Bonferroni, C.E., 1936. Teoria statistica delle classi e calcolo delle probabilita. Pubblicazioni del R Istituto Superiore di Sceinze Economiche e Commerciali di Firenze 8, pp. 3–62.
Bramen, J.E., Hranilovich, J.A., Dahl, R.E., Forbes, E.E., Chen, J., Toga, A.W., Dinov, I.D., Worthman, C.M., Sowell, E.R., 2011. Puberty influences medial temporal lobe and cortical gray matter maturation differently in boys than girls matched for sexual maturity. Cereb. Cortex 21 (3), 636–646.
Brito, N.H., Noble, K.G., 2014. Socioeconomic status and structural brain development. Front. Neurosci. 8, 276.
Bzdok, D., Laird, A.R., Zilles, K., Fox, P.T., Eickhoff, S.B., 2013. An investigation of the structural, connectional, and functional subspecialization in the human amygdala. Hum. Brain Mapp. 34 (12), 3247–3266.
Chaplin, T.M., Aldao, A., 2013. Gender differences in emotion expression in children: a meta-analytic review. Psychol. Bull. 139 (4), 735–765.
Cservenka, A., Stroup, M.L., Etkin, A., Nagel, B.J., 2015. The effects of age, sex, and hormones on emotional conflict-related brain response during adolescence. Brain Cogn. 99, 135–150.
Cunningham, M.G., Bhattacharyya, S., Benes, F.M., 2002. Amygdalo-cortical sprouting continues into early adulthood: implications for the development of normal and abnormal function during adolescence. J. Comp. Neurol. 453 (2), 116–130.
deCampo, D.M., Fudge, J.L., 2012. Where and what is the paralaminar nucleus? A review on a unique and frequently overlooked area of the primate amygdala. Neurosci. Biobehav. Rev. 36 (1), 520–535.
deCampo, D.M., Fudge, J.L., 2013. Amygdala projections to the lateral bed nucleus of the stria terminalis in the macaque: comparison with ventral striatal afferents. J. Comp. Neurol. 521 (14), 3191–3216.
Dorn, L.D., 2006. Measuring puberty. J. Adolesc. Health 39 (5), 625–626.
Fudge, J.L., deCampo, D.M., Becoats, K.T., 2012. Revisiting the hippocampal-amygdala pathway in primates: association with immature-appearing neurons. Neuroscience 212, 104–119.
Gabard-Durnam, L.J., Flannery, J., Goff, B., Gee, D.G., Humphreys, K.L., Telzer, E., Hare, T., Tottenham, N., 2014. The development of human amygdala functional connectivity at rest from 4 to 23 years: a cross-sectional study. Neuroimage 95, 193–207.
Ghashghaei, H.T., Barbas, H., 2002. Pathways for emotion: interactions of prefrontal and anterior temporal pathways in the amygdala of the rhesus monkey. Neuroscience 115 (4), 1261–1279.
Giedd, J.N., Vaituzis, A.C., Hamburger, S.D., Lange, N., Rajapakse, J.C., Kaysen, D., Vauss, Y.C., Rapoport, J.L., 1996. Quantitative MRI of the temporal lobe, amygdala, and hippocampus in normal human development: ages 4-18 years. J. Comp. Neurol. 366 (2), 223–230.
Goddings, A.L., Mills, K.L., Clasen, L.S., Giedd, J.N., Viner, R.M., Blakemore, S.J., 2014. The influence of puberty on subcortical brain development. Neuroimage 88, 242–251.
Hariri, A.R., Tessitore, A., Mattay, V.S., Fera, F., Weinberger, D.R., 2002. The amygdala response to emotional stimuli: a comparison of faces and scenes. Neuroimage 17 (1), 317–323.
Herting, M.M., Gautam, P., Spielberg, J.M., Kan, E., Dahl, R.E., Sowell, E.R., 2014. The role of testosterone and estradiol in brain volume changes across adolescence: a longitudinal structural MRI study. Hum. Brain Mapp. 35 (11), 5633–5645.
Herting, M.M., Johnson, C., Mills, K.L., Vijayakumar, N., Dennison, M., Liu, C., Goddings, A.L., Dahl, R.E., Sowell, E.R., Whittle, S., Allen, N.B., Tamnes, C.K., 2018. Development of subcortical volumes across adolescence in males and females: a multisample study of longitudinal changes. Neuroimage 172, 194–205.
Herting, M.M., Azad, A., Kim, R., Tyszka, J.M., Geffner, M.E., Kim, M.S., 2020. Brain differences in the prefrontal cortex, Amygdala, and Hippocampus in youth with congenital adrenal hyperplasia. J. Clin. Endocrinol. Metab.
Herzog, A.G., Van Hoesen, G.W., 1976. Temporal neocortical afferent connections to the amygdala in the rhesus monkey. Brain Res. 115 (1), 57–69.
Hollingshead, A.A., 1975. Four-factor Index of Social Status. Unpublished manuscript. Yale University, New Haven, CT.
Janak, P.H., Tye, K.M., 2015. From circuits to behaviour in the amygdala. Nature 517 (7534), 284–292.
Jenkinson, M., Beckmann, C.F., Behrens, T.E., Woolrich, M.W., Smith, S.M., 2012. FSL. Neuroimage 62 (2), 782–790.
Killcross, S., Robbins, T.W., Everitt, B.J., 1997. Different types of fear-conditioned behaviour mediated by separate nuclei within amygdala. Nature 388 (6640), 377–380.
Krettek, J.E., Price, J.L., 1978. A description of the amygdaloid complex in the rat and cat with observations on intra-amygdaloid axonal connections. J. Comp. Neurol. 178 (2), 255–280.
McDonald, A.J., Jackson, T.R., 1987. Amygdaloid connections with posterior insular and temporal cortical areas in the rat. J. Comp. Neurol. 262 (1), 59–77.
Meyer-Lindenberg, A., Hariri, A.R., Munoz, K.E., Mervis, C.B., Mattay, V.S., Morris, C.A., Berman, K.F., 2005. Neural correlates of genetically abnormal social cognition in Williams syndrome. Nat. Neurosci. 8 (8), 991–993.
Morales, A.M., Jones, S.A., Ehlers, A., Lavine, J.B., Nagel, B.J., 2018. Ventral striatal response during decision making involving risk and reward is associated with future binge drinking in adolescents. Neuropsychopharmacology 43 (9), 1884–1890.
Must, A., Anderson, S.E., 2006. Body mass index in children and adolescents: considerations for population-based applications. Int. J. Obes. (Lond.) 30 (4), 590–594.
Nakagawa, S., Cuthill, I.C., 2007. Effect size, confidence interval and statistical significance: a practical guide for biologists. Biol. Rev. Camb. Philos. Soc. 82 (4), 591–605.
Pauli, W.M., Nili, A.N., Tyszka, J.M., 2018. A high-resolution probabilistic in vivo atlas of human subcortical brain nuclei. Sci. Data 5, 180063.
Perlaki, G., Molnar, D., Smeets, P.A.M., Ahrens, W., Wolters, M., Eiben, G., Lissner, L., Erhard, P., Meer, F.V., Herrmann, M., Janszky, J., Orsi, G., 2018. Volumetric gray matter measures of amygdala and accumbens in childhood overweight/obesity. PLoS One 13 (10), e0205331.
Petersen, A.C., Crockett, L., Richards, M., Boxer, A., 1988. A self-report measure of pubertal status: reliability, validity, and initial norms. J. Youth Adolesc. 17 (2), 117–133.
Phillips, R.G., LeDoux, J.E., 1992. Differential contribution of amygdala and hippocampus to cued and contextual fear conditioning. Behav. Neurosci. 106 (2), 274–285.
Pintzka, C.W., Hansen, T.I., Evensmoen, H.R., Håberg, A.K., 2015. Marked effects of intracranial volume correction methods on sex differences in neuroanatomical structures: a HUNT MRI study. Front. Neurosci. 9, 238.
Pitkanen, A., Amaral, D.G., 1998. Organization of the intrinsic connections of the monkey amygdaloid complex: projections originating in the lateral nucleus. J. Comp. Neurol. 398 (3), 431–458.
Raznahan, A., Lerch, J.P., Lee, N., Greenstein, D., Wallace, G.L., Stockman, M., Clasen, L., Shaw, P.W., Giedd, J.N., 2011. Patterns of coordinated anatomical change in human cortical development: a longitudinal neuroimaging study of maturational coupling. Neuron 72 (5), 873–884.
Reppucci, C.J., Petrovich, G.D., 2016. Organization of connections between the amygdala, medial prefrontal cortex, and lateral hypothalamus: a single and double retrograde tracing study in rats. Brain Struct. Funct. 221 (6), 2937–2962.
Rollins, B.L., King, B.M., 2000. Amygdala-lesion obesity: what is the role of the various amygdaloid nuclei? Am. J. Physiol. Regul. Integr. Comp. Physiol. 279 (4), R1348–1356.
Sah, P., Faber, E.S., Lopez De Armentia, M., Power, J., 2003. The amygdaloid complex: anatomy and physiology. Physiol. Rev. 83 (3), 803–834.
Sananes, C.B., Davis, M., 1992. N-methyl-D-aspartate lesions of the lateral and basolateral nuclei of the amygdala block fear-potentiated startle and shock sensitization of startle. Behav. Neurosci. 106 (1), 72–80.
Saygin, Z.M., Kliemann, D., Iglesias, J.E., van der Kouwe, A.J.W., Boyd, E., Reuter, M., Stevens, A., Van Leemput, K., McKee, A., Frosch, M.P., Fischl, B., Augustinack, J.C., 2017. High-resolution magnetic resonance imaging reveals nuclei of the human amygdala: manual segmentation to automatic atlas. Neuroimage 155, 370–382.
Scheuer, H., Alarcon, G., Demeter, D.V., Earl, E., Fair, D.A., Nagel, B.J., 2017. Reduced fronto-amygdalar connectivity in adolescence is associated with increased depression symptoms over time. Psychiatry Res. Neuroimaging 266, 35–41.
Schoenbaum, G., Chiba, A.A., Gallagher, M., 1999. Neural encoding in orbitofrontal cortex and basolateral amygdala during olfactory discrimination learning. J. Neurosci. 19 (5), 1876–1884.
Shaffer, D., Fisher, P., Lucas, C.P., Dulcan, M.K., Schwab-Stone, M.E., 2000. NIMH Diagnostic Interview schedule for Children Version IV (NIMH DISC-IV): description, differences from previous versions, and reliability of some common diagnoses. J. Am. Acad. Child Adolesc. Psychiatry 39 (1), 28–38.
Smith, S.M., Jenkinson, M., Woolrich, M.W., Beckmann, C.F., Behrens, T.E., Johansen-Berg, H., Bannister, P.R., De Luca, M., Drobnjak, I., Flitney, D.E., Niazy, R.K., Saunders, J., Vickers, J., Zhang, Y., De Stefano, N., Brady, J.M., Matthews, P.M., 2004. Advances in functional and structural MR image analysis and implementation as FSL. Neuroimage 23 (Suppl 1), S208–219.
Solano-Castiella, E., Schafer, A., Reimer, E., Turke, E., Proger, T., Lohmann, G., Trampel, R., Turner, R., 2011. Parcellation of human amygdala in vivo using ultra high field structural MRI. Neuroimage 58 (3), 741–748.
Stan, A.D., Ghose, S., Gao, X.M., Roberts, R.C., Lewis-Amezcua, K., Hatanpaa, K.J., Tamminga, C.A., 2006. Human postmortem tissue: what quality markers matter? Brain Res. 1123 (1), 1–11.

Tosevski, J., Malikovic, A., Mojsilovic-Petrovic, J., Lackovic, V., Peulic, M., Sazdanovic, P., Alexopulos, C., 2002. Types of neurons and some dendritic patterns of basolateral amygdala in humans–a golgi study. Ann. Anat. 184 (1), 93–103.
Tottenham, N., Gabard-Durnam, L.J., 2017. The developing amygdala: a student of the world and a teacher of the cortex. Curr. Opin. Psychol. 17, 55–60.
Tustison, N.J., Avants, B.B., Cook, P.A., Zheng, Y., Egan, A., Yushkevich, P.A., Gee, J.C., 2010. N4ITK: improved N3 bias correction. IEEE Trans. Med. Imaging 29 (6), 1310–1320.
Tyszka, J.M., Pauli, W.M., 2016. In vivo delineation of subdivisions of the human amygdaloid complex in a high-resolution group template. Hum. Brain Mapp. 37 (11), 3979–3998.
Wan, F.J., Swerdlow, N.R., 1997. The basolateral amygdala regulates sensorimotor gating of acoustic startle in the rat. Neuroscience 76 (3), 715–724.
Wierenga, L., Langen, M., Ambrosino, S., van Dijk, S., Oranje, B., Durston, S., 2014. Typical development of basal ganglia, hippocampus, amygdala and cerebellum from age 7 to 24. Neuroimage 96, 67–72.
Wierenga, L.M., Bos, M.G.N., Schreuders, E., Vd Kamp, F., Peper, J.S., Tamnes, C.K., Crone, E.A., 2018. Unraveling age, puberty and testosterone effects on subcortical brain development across adolescence. Psychoneuroendocrinology 91, 105–114.
Wierenga, L.M., Doucet, G., Dima, D., Agartz, I., Aghajani, M., Akudjedu, T.N., Albajes-Eizagirre, A., AlnÊs, D., Alpert, K., Andreassen, O.A., Anticevic, A., Asherson, P., Banaschewski, T., BargallÛ, N., Baumeister, S., Baur-Streubel, R., Bertolino, A., Bonvino, A., Boomsma, D., Borgwardt, S., Bourque, J., Braber, Ad., Brandeis, D., Breier, A., Brodaty, H., Brouwer, R., Buitelaar, J., Busatto, G., Calhoun, V., Canales-RodrÌguez, E.J., Cannon, D., Caseras, X., Castellanos, F.X., Chaim-Avancini, T., Ching, C., Clark, V., Conrod, P., Conzelmann, A., Crivello, F., Davey, C., Dickie, E., Ehrlich, S., Ent, Dvt., Fisher, S., Fouche, J., Franke, B., Fuentes-Claramonte, P., Geus, E.Dd., Giorgio, A.D., Glahn, D., Gotlib, I., Grabe, H., Gruber, O., Gruner, P., Gur, R., Gurholt, T., Haan, Ld., Haatveit, B., Harrison, B., Hartman, C., Hatton, S., Heslenfeld, D., Heuvel, O.Avd., Hickie, I., Hoekstra, P., Hohmann, S., Holmes, A., Hoogman, M., Hosten, N., Howells, F., Pol, H.H.H., Huyser, C., Jahanshad, N., James, A., Jiang, J., Jnsson, E., Joska, J., Kalnin, A., Klein, M., Koenders, L., KolskÅr, K.K., Kr‰mer, B., Kuntsi, J., Lagopoulos, J., Lazaro, L., Lebedeva, I., Lee, P., Lochner, C., Machielsen, M., Maingault, S., Martin, N., MartÌnez-ZalacaÌn, I., Mataix-Cols, D., Mazoyer, B., McDonald, B., McDonald, C., McIntosh, A., McMahon, K., McPhilemy, G., Meer, Dvd., MenchÛn, J., Naaijen, J., Nyberg, L., Oosterlaan, J., Paloyelis, Y., Pauli, P., Pergola, G., Pomarol-Clotet, E., Portella, M., Radua, J., Reif, A., Richard, G., Roffman, J., Rosa, P., Sacchet, M., Sachdev, P., Salvador, R., SarrÛ, S., Satterthwaite, T., Saykin, A., Serpa, M.H., Sim, K., Simmons, A., Smoller, J. W., Sommer, I., Soriano-Mas, C., Stein, D., Strike, L., Szeszko, P., Temmingh, H., Thomopoulos, S.I., Tomyshev, A., Trollor, J., Uhlmann, A., Veer, I., Veltman, D., Voineskos, A., Vlzke, H., Walter, H., Wang, L., Wang, Y., Weber, B., Wen, W., West, J., Westlye, L., Whalley, H., Williams, S., Wittfeld, K., Wolf, D., Wright, M.J., Yoncheva, Y., Zanetti, M., Ziegler, G.C., Zubicaray, G.Dd., Thompson, P., Crone, E., Frangou, S., Tamnes, C.K., 2020. Greater male than female variability in regional brain structure across the lifespan. bioRxiv.
Woolrich, M.W., Jbabdi, S., Patenaude, B., Chappell, M., Makni, S., Behrens, T., Beckmann, C., Jenkinson, M., Smith, S.M., 2009. Bayesian analysis of neuroimaging data in FSL. Neuroimage 45 (1 Suppl), S173–186.